AN ABSTRACT OF THE DISSERTATION OF

Hattan Natto for the degree of Doctor of Philosophy in Radiation Health Physics presented on November 17, 2021.

Title: Cherenkov Glass Detectors for Gamma and Neutron Detection.

Abstract approved:

_____

Dr. Haori Yang

Cherenkov detectors have been developed and used in several fields since the discovery of Cherenkov radiation. They do have several advantages compared with other detector types, such as low noise due to the low-energy threshold of Cherenkov radiation, and short decay constant (on the order of picoseconds). However, the light yield of Cherenkov detectors is low. Only several hundreds of Cherenkov photons can be generated per MeV. The objective of this work is to manufacture and test Cherenkov glass detectors for detection of high energy gammas and neutrons. ^{60}Co was used for gamma ray measurements, and PuBe source was used for neutrons measurements. Gd_2O_3 was used as an activator to capture thermal neutrons. As a result of this capture, gamma rays were generated and interacted with Cherenkov detectors to produce Cherenkov light. The focus was to improve the light output of Cherenkov detectors by adding high Z materials and implementing Wavelength Shifting (WLS) fibers inside the glass samples. Increasing the Z number of the glass samples increases the interaction probability, and without the WLS materials, most Cherenkov photons are likely to be absorbed within the glass sample before they could reach the photon sensor. WLS fibers do not directly increase the number of Cherenkov photons, but they can reduce the energy of Cherenkov photons and direct them towards the photon sensor. A Geant4 simulation toolkit was used to create a detailed model, and to understand and confirm that the measured observations were reasonable.

©Copyright by Hattan Natto
November 17, 2021
All Rights Reserved

Cherenkov Glass Detectors for Gamma and Neutron Detection

by
Hattan Natto

A DISSERTATION

submitted to

Oregon State University

in partial fulfillment of
the requirements for the
degree of

Doctor of Philosophy

Presented November 17, 2021
Commencement June 2022

Doctor of Philosophy dissertation of Hattan Natto presented on November 17, 2021

APPROVED:

Major Professor, representing Radiation Health Physics

Head of the School of Nuclear Science and Engineering

Dean of the Graduate School

I understand that my dissertation will become part of the permanent collection of Oregon State University libraries. My signature below authorizes release of my dissertation to any reader upon request.

Hattan Natto, Author

ACKNOWLEDGEMENTS

During my graduate study at Oregon Stata University, I have encountered some exciting, intense, and joyful time. This period of time was truly unique and memorable. Here I would like to take my chance and thank all the people who supported me during my study journey since it would not be possible for me to make it without their help and support.

First, I would like to thank my major advisor, Dr. Haori Yang, for his support and encouragement for my education and research. During my work on Cherenkov radiation detectors, he advised me through the project until the end. I have built a strong background in radiation detection and measurement, producing Cherenkov glass detectors, and running Geant4 simulation. Even though 2020 was an unusual year for majority of us due to an abundance of caution regarding the spread of the COVID-19 pandemic, Dr. Yang would not hesitate and was always there to help and support me. He was available anytime I needed him to discuss any issues I was facing in my research work. His experience and knowledge about radiation detection and measurements provided precious supervision for my PhD research work. I was so fortunate and lucky to have Dr. Yang as my major advisor and cannot thank him more for what he has done for me.

Also, I would take the chance to thank Dr. Abi Farsoni, Dr. Steven Reese, Dr. Camille Palmer, and Dr. Kenneth Krane for being my committee members. Finally, I would like to thank my parents, my siblings, my wife, and my kids. Their love and support were essential to finishing my study.

Table of Contents

LIST OF FIGURES

LIST OF FIGURES (Continued)

LIST OF TABLES

1 Introduction

Cherenkov radiation is a phenomenon that takes place when an energetic charged particle's speed exceeds the phase velocity of light in a medium and interacts with the medium's molecules to generate photons with wavelengths in the range of the violet color. Since the discovery of Cherenkov radiation by Pavel Cherenkov in 1934 [1,2], Cherenkov detectors have been developed and used in different fields, such as astrophysics experiments, radiochemistry and biology [3]. Also, several Cherenkov detector applications have been reported, like Ring Imaging Cherenkov (RICH) detectors [4], Time-Of-Flight Positron Emission Tomography (PET) applications [5], detection of antineutrino by neutron sensing [6], threshold discrimination and particle identification [7,8], and X-ray imaging systems [9,10]. One important application detects special nuclear materials (SNM) by using the Time-Of-Flight technique. Cargo can be induced and interrogated by using a high energy beam; then Cherenkov detectors detect the characteristic radiations of specific SNM [11]. Moreover, several types of Cherenkov detectors have been reported including water [12-14], silica aerogel [15,16], gas [17,18], and glass [19-22]. The most extensively studied and used is the glass type, especially lead glass [23-25] because of the high refractive index (n) and density.

The yield of Cherenkov photons generated in a medium is a function of wavelength, and it is proportional to $1/\lambda^2$. Therefore, the emission concentrates in the short-wavelength region of the spectrum. In the case of extremely short wavelengths, the number of Cherenkov photons ultimately falls back because the refractive index as

a function of wavelength approaches unity [26]. The yield of Cherenkov photons *dN* per unit length *dx* can be calculated by [27]:

$$\frac{dN}{dx} = 2\pi\alpha\left(\frac{1}{\lambda_1} - \frac{1}{\lambda_2}\right) sin^2\theta$$
$$sin^2\theta = \left(1 - \frac{1}{(vn/c)^2}\right) \quad (1)$$

where α is the fine structure constant (1/137); λ_1 is the lower wavelength of the Cherenkov emission band and λ_2 is the upper wavelength of the Cherenkov emission band; θ is the half angle of emitted Cherenkov lights; *n* is the refractive index; and v is the velocity of the particle.

Generally, in order to generate Cherenkov photons in a given medium, the following condition should be achieved:

$$1 < \beta n \quad (2)$$

where β is the fraction of the speed of the charged particle $\nu_{particle}$ in the medium to that of light in a vacuum ($c = 3\times10^8$ m/s) and n is the refractive index of the medium. The refractive index is the ratio between the speed of light in vacuum to speed of light in medium c_{medium}.

$$\beta = \frac{\nu_{particle}}{c} \quad \text{and} \quad n = \frac{c}{c_{medium}} \quad (3)$$

By multiplying βn, we get:

$$1 < \frac{v_{particle}}{c_{medium}} \tag{4}$$

The above condition shows a minimum particle speed is required to produce Cherenkov radiation. Additionally, the half angel of emitting Cherenkov radiations θ can be calculated by:

$$\cos\theta = \frac{1}{\beta n} = \frac{c_{medium}}{v_{particle}} \tag{5}$$

Cherenkov detectors only respond to the radiation which is capable of generating energetic electrons that can exceed the speed of light in the medium. In other words, the incident radiation should have a minimum energy in order to generate Cherenkov photons. The threshold energies as a result of photoelectric effect and Compton scattering can be calculated by [28]:

$$E_{th\_photoelectric} = m_0c^2\left(-1 + \sqrt{1 + \frac{1}{n^2 - 1}}\right) \tag{6}$$

$$E_{th\_compton} = \frac{1}{2}m_0c^2\left(-1 + \sqrt{1 + \frac{1}{n^2 - 1}}\right)\left(1 + \sqrt{1 + \frac{2}{\frac{n}{\sqrt{n^2 - 1}} - 1}}\right) \tag{7}$$

where m_0c^2 is the electron rest mass energy (0.511 MeV). Figure 1.1 shows the relationship between the threshold energy (as a result of photoelectric effect and

Compton scattering) and the speed of light as a function of their refractive index. A higher refractive index results in a lower threshold energy and speed of light.

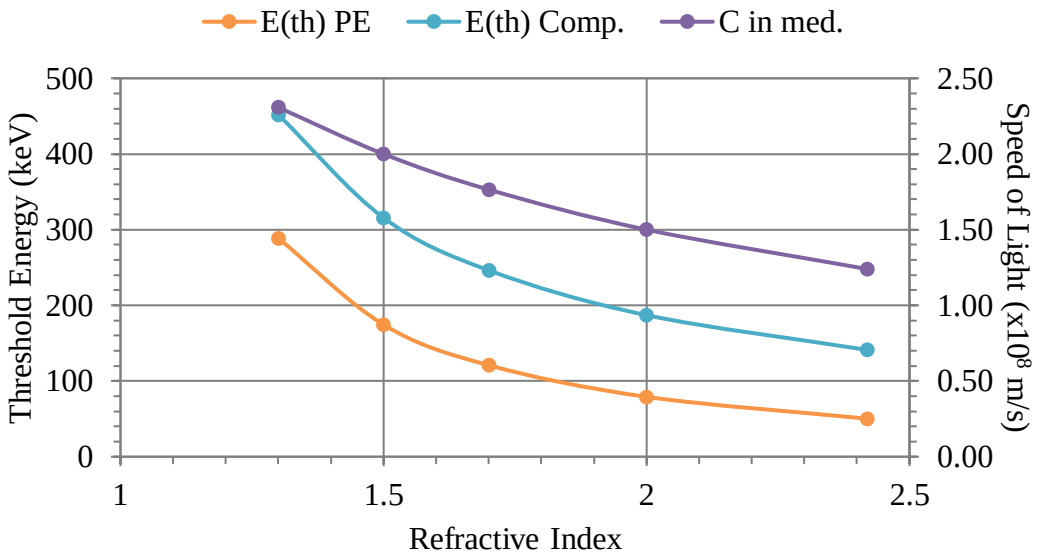

Figure 1. 1The threshold energies and the speed of light as a function of the refraction index.

Cherenkov detectors produce light output for easy detection using common photon sensors. In addition, they have several advantages compared with other detector types, such as producing low noise due to the low-energy threshold of Cherenkov radiation and short decay constant (on the order of picoseconds), which make Cherenkov detectors remarkably fast. However, the light yield of Cherenkov radiation is low. Figure 1.2 demonstrates that only several hundred of Cherenkov photons could be generated per MeV. That means about 10^{-3} of the particle's energy is converted into visible light [26].

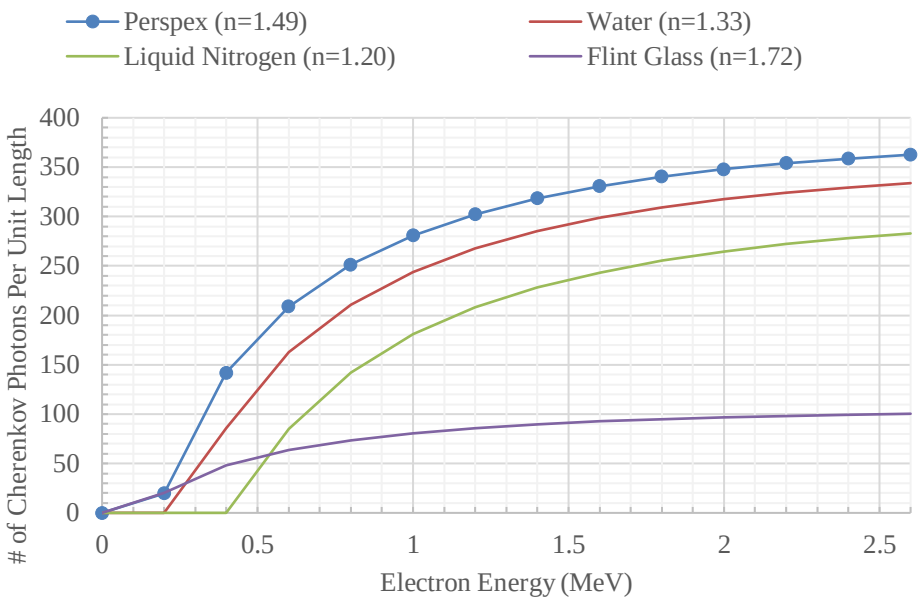

Figure 1. 2 Calculated number of Cherenkov photons in the 300-600 nm wavelength range for several detection media by using equation (1).

The objective of this work is to produce and test Cherenkov glass detectors for detection of gamma and neutron rays. The focus is to improve the light output of Cherenkov detectors and make them more efficient by adding rare earth elements to the glass and incorporate the Wavelength Shifting (WLS) fibers. The purpose of having rare earth elements in the composition of the glass samples is to increase the probability of interaction between the incident gamma rays and the detector. The WLS fibers have the ability to shift the spectrum of the Cherenkov radiation towards longer wavelength, reduce the number of Cherenkov photons absorbed by the glass, and improve coupling with the Photomultiplier Tube. A Geant4 simulation toolkit was used to create a detailed model and to understand and confirm that the measured observations were reasonable.

References

[1] P. A. Cherenkov, “Visible light from clear liquids under the action of gamma radiation,” Dokl Akad Nauk SSSR 2:451, 1934.

[2] S. I. Vavilov “On possible causes of dark blue radiation in liquids,” Dokl Akad Nauk SSSR 2:457, 1934.

[3] P (ed). Carlson “Cherenkov detectors and their applications in science and technology,” *Nucl. Instrum. Methods* A 248, 1986.

[4] I. Iijima, et al., “Studies of a proximity focusing aerogel RICH for future Belle upgrade,” *Nucl. Inst. Meth.* A 595:92–95, 2008.

[5] S. Korpar, R. Dolenec, P. Krizan, R. Pestotnik, A. Stanovnik, “Study of TOF PET using Cherenkov light,” *Nucl Instrum Methods* A 654:532–538, 2011.

[6] P. Lecoq, et al., “Factors influencing time resolution of scintillators and ways to improve them,” *IEEE Trans Nucl Sci* 57:2411–2416, 2010.

[7] T. Iijima, et al., “Studies of a proximity focusing RICH with aerogel radiator for future Belle upgrade,” *Nucl Instrum Methods* A 595:92–95, 2008.

[8] P. Cenci, et al., “The ring imaging Cherenkov detector of the NA62 experiment at CERN,” *Nucl Instrum Methods* A 732:342–345, 2013.

[9] A. Anatoli, M. A. Billercia, “Scintillation-Cherenkov detector and method for high energy X-ray cargo container imaging and industrial radiography,” US Patent US 2011/0163236 A1, 2011.

[10] G. G. Pang, J. A. Rowlands, “Cherenkov X-ray detector for portal imaging,” US Patent US7297914 B2, 2007.

[11] Erickson A S., “Remote Detection of Fissile Material: Cherenkov Counters for Gamma Detection,” Ph.D. dissertation, Massachusetts Institute of Technology, 2011.

[12] M. Sweany, A. Bernstein, N. Bowden, S. Dazeley, R. Svoboda, “Special nuclear detection with water Cherenkov based detectors,” *IEEE NSS Conf. Record*, N61-5:3372-3375. Dresden, Germany, 2008.

[13] S. Dazeley, M. Sweany, A. Bernstein, "SNM detection with an optimized Cherenkov neutron detector," *Nucl Instrum Methods* A 693:148–153, 2012.

[14] H. W. Button-Shafer Churchill, R. L. Lichti, D. H. Novack, "Development of a large low-mass, water Cherenkov counter," *Nucl Instrum Methods* 137:29–40, 1976.

[15] R. Pestotnik, S. Korpar, P. Krizan, R. Dolenec, "Cherenkov detector of 90Sr on aerogel as radiator," *Nucl Instrum Methods* A 595:278–280, 2008.

[16] S. Nishida, et al., "Development of a 144-channel Hybrid Avalanche Photo-detector for Belle II ring-imaging Cherenkov counter with aerogel radiator," *Nucl Instrum Methods* A 787:59–63, 2015.

[17] M. Iodice, et al., "The CO2 gas Cherenkov detectors for the Jefferson Lab Hall—a spectrometer," *Nucl Instrum Methods* A 411:223–237, 1998.

[18] D. Hampf, M. Tluczykont, D. Horns, "Event reconstruction techniques for the wide-angle air Cherenkov detector HiSCORE," *Nucl Instum Methods* A 712:137–146, 2013.

[19] Z. W. Bell, L. A. Boatner "Neutron detection via the Cherenkov effect," *IEEE Trans Nucl Sci* 57:3800–3806, 2010.

[20] P. D. Grannis, D. Jaffe, M. D. Marx, "Low-cost glass Cherenkov detectors," *Nucl Instum Methods* 188:239–242, 1981.

[21] Y. Miyazaki, et al., "Performance test of lead-glass counter for the J-PARC E36 experiment," *Nucl Instrum Methods* A 779:13–17, 2015.

[22] M. Kobayashi, S. Sugimoto, U. Usuki, "Radiation hardness of PbWO4 Cherenkov radiators heavily doped with trivalent rare-earth ions," *Nucl Instrum Methods* A 524:385–389, 2004.

[23] F. Kocak, I. Tapan, "$PbWO_4$ Cherenkov light contribution to Hamamatsu S81148 and zinc sulfide-silicon avalanche photodiodes signals," *Nucl Instrum Methods* A 617:398–399, 2010.

[24] M. Kobayashi, et al., "A beam of PbWO4 Cherenkov radiators," *Nucl Instrum Methods* A 484:140–148, 2002.

[25] N. Akchurin, et al., “Contribution of Cherenkov light to the signals from lead tungstate crystals,” *Nucl Instrum Methods* A 582:474–483, 2007.

[26] G. Knoll, “Radiation detection and measurement,” *New York: Wiley*, 3rd edition, p.713, 2000.

[27] B. Ayaz-Maierhafer, et al., “Sensing of ^{252}Cf fission gamma rays using same-size glass detectors,” *J Radioanal Nucl Chem.*, Vol. 308, p. 919–926, November 2015.

[28] Z. W. Bell, and L. A. Boatner, “Neutron Detection via the Cherenkov Effect,” *IEEE TNS*, Vol. 57, NO. 6, p. 3800-3806, 2010.

2 Literature Review

2.1 Detecting of Fission Gamma Rays

Recently, Cherenkov glass detectors have been fabricated and evaluated for the detection of gamma rays [29–33]. Cherenkov glass detectors have advantages over other detectors in discriminating low-energy photons, handling high counting rate, and performing timing coincidence or photon time-of-flight measurements. The photon time-of-flight measurement allows investigation of MeV photons emission from a specific target. Cherenkov glass detectors were investigated to detect prompt gammas from induced fission when depleted uranium was exposed to short pulses of 6, 10, and 25 MeV bremsstrahlung beams [32]. The experimental setup for this study is shown in Figure 2.1.

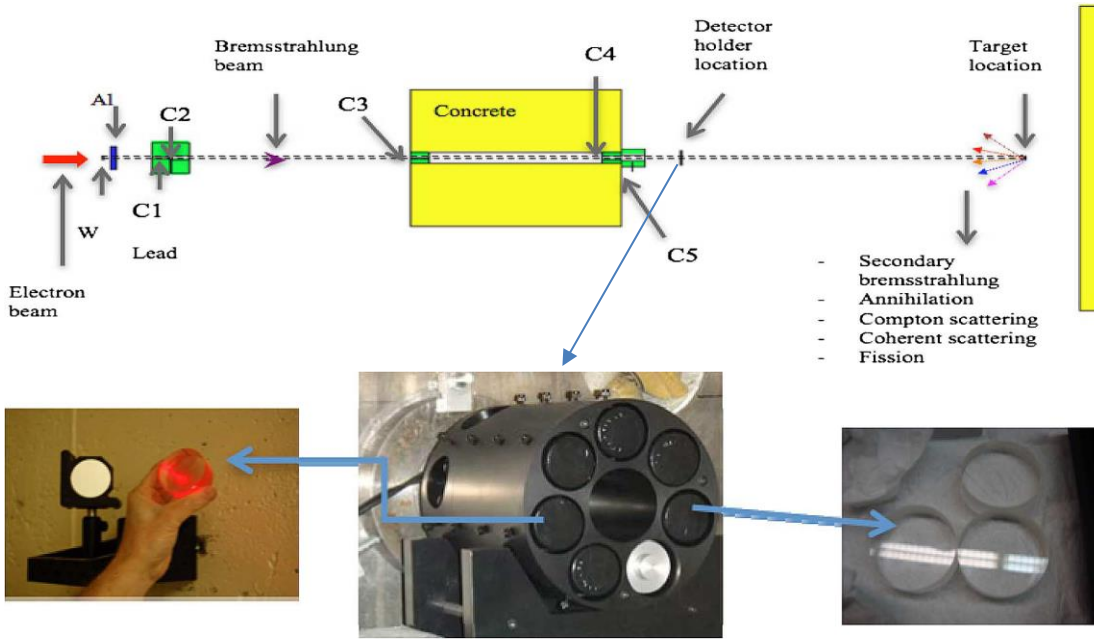

Figure 2. 1 Experimental setup to detect prompt gammas from induced fission [32].

The bremsstrahlung beam passed through several collimators, a concrete wall, and the detector holder before hitting the target. When the primary beam hits the target,

a number of photon interactions within the target may result in producing high energy radiation such as secondary bremsstrahlung, annihilation photons, Compton scattering, Coherent scattering, and fission gamma rays. The result from this study shows that Cherenkov glass detectors were not able to sense the prompt fission gammas from the depleted uranium. Yet, they were able to detect the prompt fission gammas plus different series of photon interactions and secondary bremsstrahlung production within the depleted uranium as shown in Figure 2.2 [32].

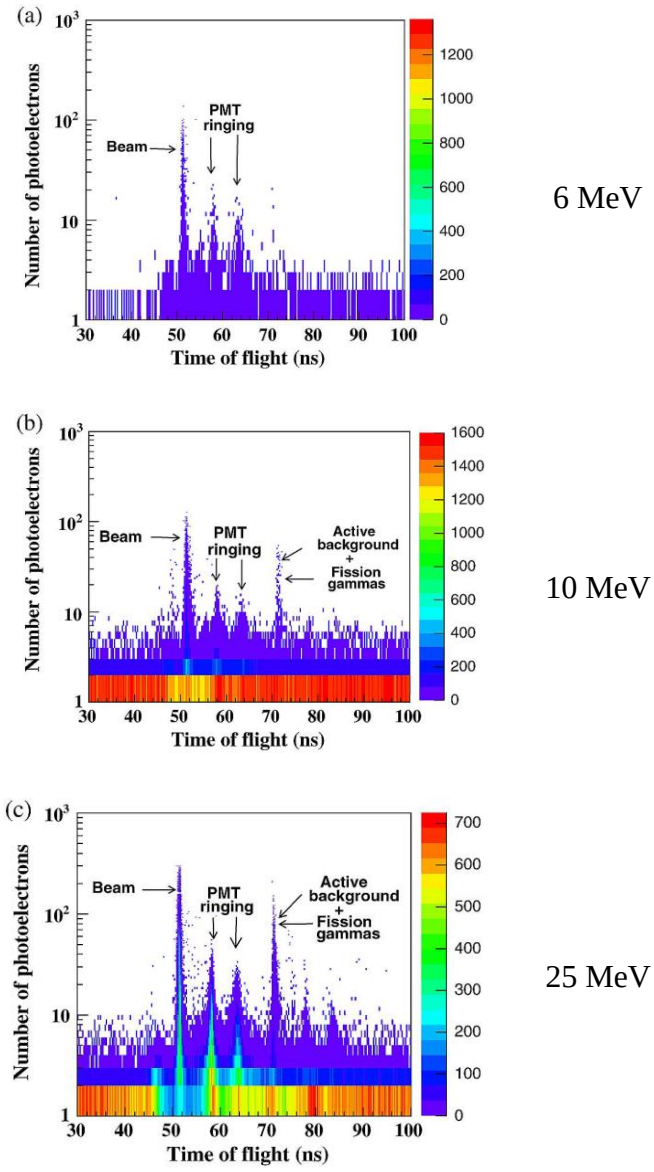

Figure 2. 2 The number of photoelectrons vs. TOF.

The results from this study led the same team to assume that the detection efficiency of the Cherenkov glass detectors depends on the physical characteristics of the glass and is complicated to quantify using fission gamma rays because of the low gamma energy and poor Cherenkov light output. Therefore, Maierhafer et. al have studied the efficiency of glass Cherenkov detectors with ^{252}Cf fission gammas [34]. The spontaneous fission decay mode of ^{252}Cf represents only 3% of the overall decay. The average energy of the prompt fission gamma rays is about 0.87 MeV with around 8 photons emitted per fission. The experimental setup of this work is shown in Figure 2.3.

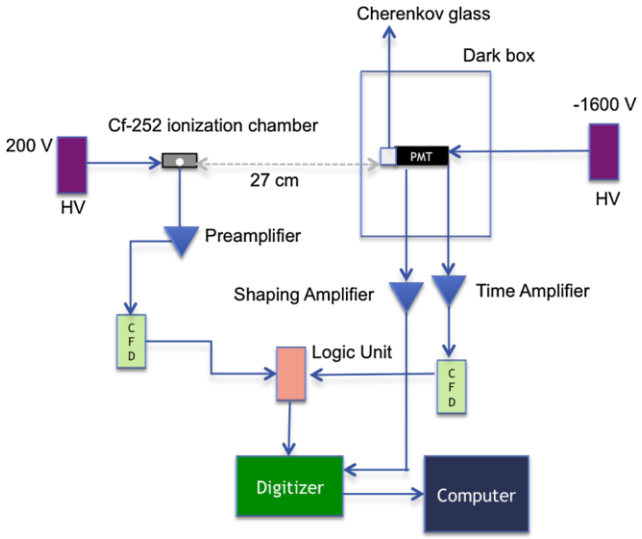

Figure 2. 3 The experimental setup of Maierhafer et. al work [34].

The focus of this investigation was on the effect of absorption edge, density, and threshold energy of glass samples. Table 2.1 shows the properties of the glass samples the authors studied in their work. There are three main factors that affect the production and collection of Cherenkov radiation:

1- The range of the electron in the medium controls the number of Cherenkov photons.

2- The refractive index of the medium affects the threshold energy.

3- Cherenkov photon collection is relied on the absorption edge of the medium.

Table 2. 1 The physical characteristics of glass samples used in [34]

No.	Glass sample	Dia/thick (mm)	Density (g/cm3)	n (600 nm)	Absorption edge (nm)	Gamma threshold (keV) ($Eth_{compton}/Eth_{pe}$)
1	Fused silica	51/36	2.2	1.45	190	341/195
2	N-SF11	51/36	3.22	1.78	383	227/107
3	N-SK5	51/36	3.3	1.59	315	280/146
4	N-LAF7	51/36	3.73	1.75	379	234/112
5	N-LAK22	51/36	3.77	1.65	326	260/131
6	N-LAF34	51/36	4.24	1.77	325	229/108
7	SF-57	51/36	5.51	1.85	379	212/96
8	PbF_2	51/36	7.77	1.82	290	218/101
9	MgCs phosphate	55/30	3.15	1.54	240	299

Their results showed how the detecting efficiency is affected by density and the absorption edge of the glass samples. Even though high density increases the probability of interaction, it would reduce the path of the electron which leads to the reduction of the number of Cherenkov photons generated. The most important factor among the three was the optical absorption edge since the counts per second is increased as the absorption edge is decreased, as shown in Figure 2.4 [34].

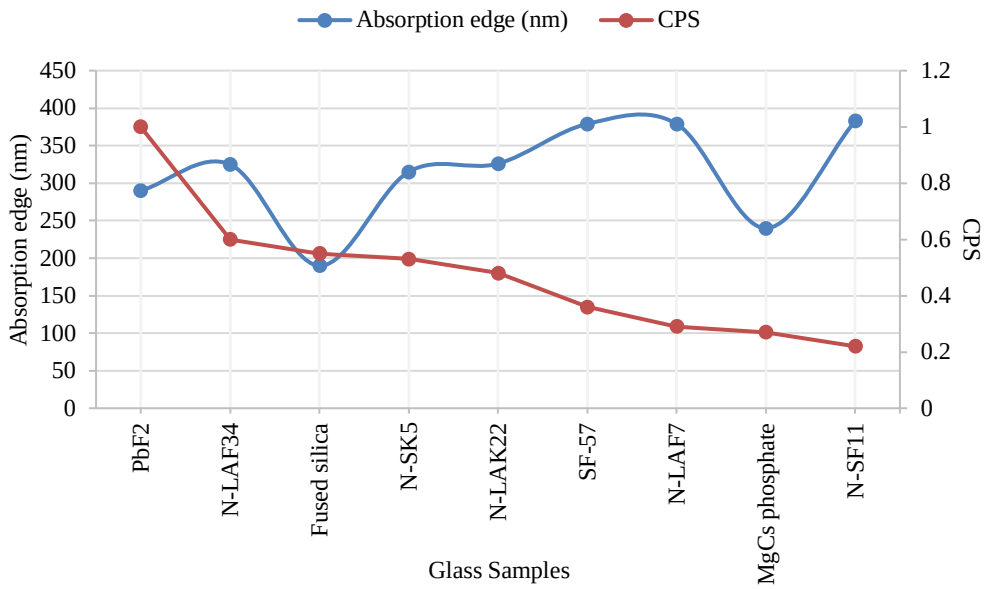

Figure 2. 4 The relationship between the absorption edge and counts per second (CPS).

2.2 Cherenkov Glass Detectors Response to Radioisotope Sources

Low-energy gamma rays from radioisotope sources have been tested on three Cherenkov glass detectors by Hayward et al. [35]. The reported efficiency for gamma ray detection was low since the glass samples were not thick enough. Table 2.2 shows the physical properties of the three glass samples and their compositions. Generally, the efficiency of gamma ray detection depends on some factors such as density, Z_{eff}, and size. Even though the glass samples had high densities and Z_{eff}, they had small thicknesses. High efficiency detection of low-energy gamma-rays needs to have thick Cherenkov glass detectors to achieve reasonable detection efficiency.

Table 2. 2 The physical characteristics of the glass samples.

Glass	Density (g/cc)	n (600 nm)	Thick/dia (mm)	Z_{eff}	E_{th} (keV)	Materials
A	2.83	1.56	1.47 /51.2	33.7	155	90g cl glass frit + 7.2 g In_2O_3
B	4.57	1.72	7.8 /50.8	61.3	117	90g PbP_2O_5 + 3.6g Sc_2O_3
C	3.86	1.7	13.7/51.1	50.2	121	90g ZnB glass frit + 22.5g Lu_2O_3

Measurement of Cherenkov lights produced by low energy gamma-ray from ^{22}Na and ^{54}Mn in the glass samples with PMTs was difficult due to the interference of natural radiation background such as ^{40}K. Even though the noise and background radiation are mixed with the gamma ray response, the separation increases when higher energy gamma rays were used (i.e. a moderated PuBe source). The efficiency of light collection affects the absolute count rate when measuring low energy photons from isotopic sources because the Cherenkov events tend to occur at the single photoelectron level. The difference in light collection efficiency between glass A and C when measuring the pulse height distributions as shown in Figure 2.5 was mostly because of the difference in optical attenuation: Glass A had a lower optical attenuation than glass C.

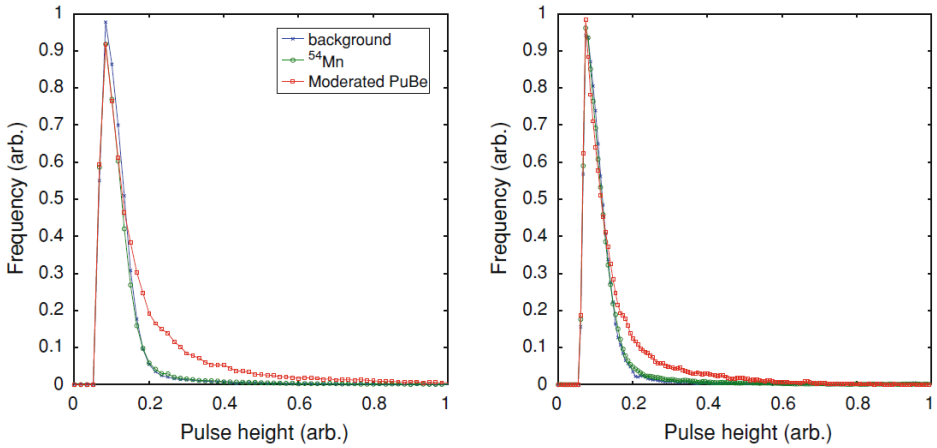

Figure 2. 5 The pulse height distributions for two types of Cherenkov glass samples. Glass A to the left and glass C to the right.

2.3 Spectra of Neutron and Gamma Ray

H. R. Vega-Carrillo and his team measured neutron and gamma ray spectra from two isotropic neutrons sources [36]. The two sources were ^{239}PuBe and ^{241}AmBe, and their activities were 5 Ci and 0.1 Ci, respectively. The neutron spectra from both sources were measured by a Bonner spheres spectrometer (BSS), while the gamma ray spectra were measured by NaI(Tl) with a neutron shield located between the sources and the detector to avoid scintillator activation. A spectrum of gamma ray background was measured as well. Figure 2.6 shows both spectra. The neutron spectra for both sources show a high peak at energies between 4 to 5 MeV and the maximum energy about 11 MeV. The gamma spectra show several significant peaks at 4.4, 3.9, and 3.4 MeV. The decay of the excited state of ^{12}C* from the ^{9}Be(n,α)^{12}C* nuclear reaction produces the 4.4 MeV peak. The 3.9 and 3.4 MeV are the single and double escape of the 4.4 MeV gamma.

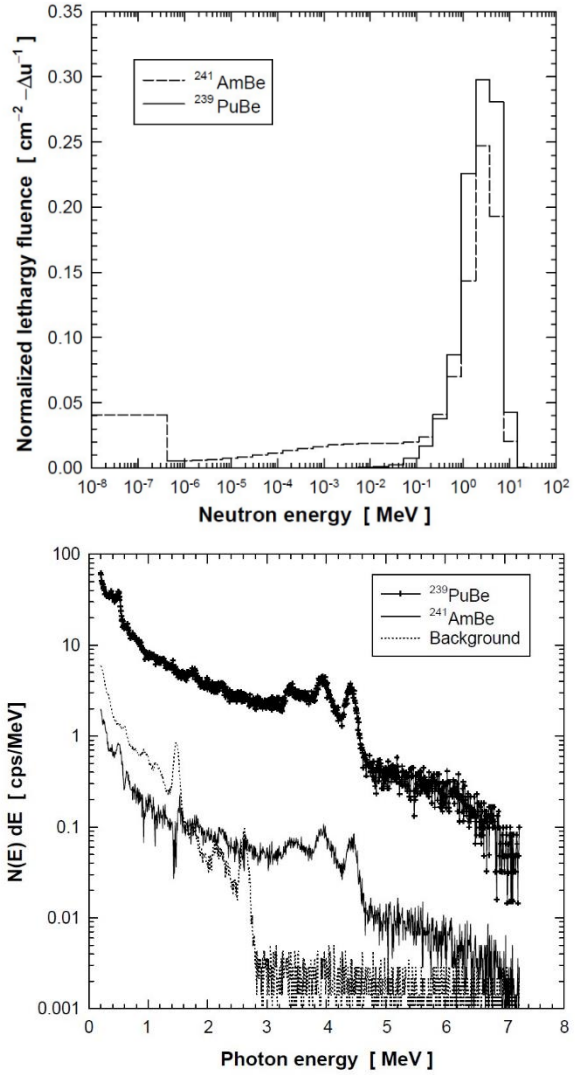

Figure 2. 6 Measured neutron and gamma ray spectra by H. R. Vega-Carrillo et al.

References

[29] B. Ayaz-Maierhafer, et al., "Measurement of thermal neutron response in Cherenkov glasses designed for MeV photon detection," *IEEE Trans Nucl Sci* 60:701–707, 2013.

[30] J. P. Hayward, et al., "Characterization the radiation response of Cherenkov glass detectors with isotopic sources," *J Radioanal Nucl Chem* 295:1143–1151, 2013.

[31] J. P. Hayward, et al., "Simulated response of Cherenkov glass detectors to MeV photons," *J Radioanal Nucl Chem* 295:1321–1329, 2013.

[32] B. Ayaz-Maierhafer, et al., “Investigation of active background from photofission in depleted uranium using Cherenkov detectors and gamma ray time-of-flight analysis,” *IEEE Trans Nucl Sci* 61:2402–2409, 2014.

[33] X. Zhang, J. P. Hayward, M. A. Laubach, “New method to remove the electronic noise for absolutely calibrating low gain photomultiplier tubes with a higher precision,” *Nucl Instrum Methods* A 755:32–37, 2014.

[34] B. Ayaz-Maierhafer, M. Laubach and J. Hayward, "Sensing of ^{252}Cf fission gamma rays using same-size glass detectors," *Journal of Radioanalytical and Nuclear Chemistry*, vol. 308, no. 3, pp. 919-926, 2015.

[35] J. Hayward et al., "Characterizing the radiation response of Cherenkov glass detectors with isotopic sources", *Journal of Radioanalytical and Nuclear Chemistry*, vol. 295, no. 2, pp. 1143-1151, 2012. Available: 10.1007/s10967-012-1898-4.

[36] H. R. Vega-Carrillo, et al., “Neutron and gamma-ray spectra of ^{239}PuBe and ^{241}AmBe,” *Applied Radiation and Isotopes*, vol. 57, pp. 167-170, 2002.

3 Materials and Methods

This chapter describes the production of Cherenkov glass detectors, the way to implement WLS fibers in the glass samples, characteristics of the used PMT, and the detection setup for gamma and neutron measurements.

3.1 Production of Cherenkov Glass Detectors

Glass making is an important phase in this work. Cherenkov glass detectors need to be crafted under particular conditions and require several tools. The following sections describe the setup used to produce Cherenkov glass samples in our lab.

3.1.1 Furnace

A Mellen MICROTHERM MS BOX furnace (shown in Figure 3.1) was used in this work for glass making. It is designed to operate safely up to 1550°C in air. The interior structure of the furnace contains a double-wall shell separated by a fan-cooled air space in order to cool down the furnace appropriately. It comes with a door interlock switch to safely interrupt power to the furnace. Also, a thick insulated door protects the operator and prevents heat loss. A single vent port is located in the top back wall of the furnace along with two gas ports for gas-in and gas-out capability. The furnace uses Silicon Carbide heating elements located on two sides of the internal chamber (three on each side). The dimensions of the heating chamber are 6” (Width) by 7” (Height) by 6” (Depth). The system of the furnace can be controlled by integrated dual-display controllers by WEST and Omega, along with a built-in integrated over temperature alarm. The WEST controller is for over-temperature conditions. So, should the furnace heat up over a certain set point for any reason (in this case 1550°C as the maximum temperature of the furnace), the controller will remove power from the furnace to limit

the risk of any damage occurring to the furnace. Once the WEST controller is setup correctly, no further settings need to be set in the controller. Further, the Omega controller can be used

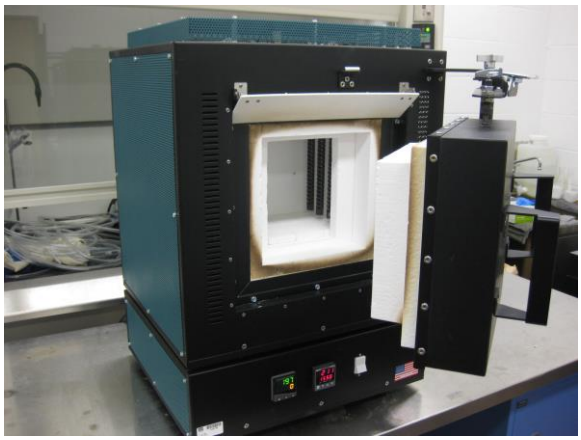

Figure 3. 1 The box furnace.

for setting temperature set point. On the Omega controller display, there are two numbers, one in orange and the other in green. The lower number in orange shows the set point temperature, and the upper number in green tells the current temperature inside the heating chamber because it is attached to a type B thermocouple. Generally, the thermocouples are temperature sensors composed of two different metals fused together that produce a change in voltage when heated. This change in voltage is interpreted as a change in temperature. Type B thermocouples are highly accurate at higher temperatures for measuring temperatures up to 1700°C. This accuracy and stability come from a relatively low millivolt output compared to other thermocouples. Unfortunately, due to low voltage output, the type B thermocouple is not reliable below approximately 600°C. In order to use the Omega controller with a type B thermocouple, the furnace must first be manually powered and controlled until the lower threshold of

the readout is reached (around 150°C) by applying 25% of the power to the system. Once the furnace reaches 150°C, the desired temperature can be set.

3.1.2 Glass Making

To obtain glass samples, first, the powdered glass ingredients were weighed on a digital scale, mixed in an alumina crucible, and melted in the box furnace for a certain time at temperatures. The volume of the alumina crucible was 100 mL, and it perfectly fit 100 g of the raw materials, enough to produce a 3 cm thick glass.

During the melting of the glass-raw material phase, raising the temperature gradually allowed the glass ingredients to be melted appropriately. Table 3.1 shows the distribution of temperatures during the melting and annealing process.

Table 3. 1 Temperatures Distribution During Glass Making

Temperature	200°C	500°C	1000°C	1400°C	1400°C to 100°C
Time	10 min	10 min	10 min	1 hour	~8 hours

After reaching the maximum temperature (1400°C), the molten ingredients were held at that temperature for 1 hour. During this hour, the ingredients melted and the sample was removed from the furnace and placed in a preheated (~ 450°C) Boron Nitride (BN) mold. The dimensions of the used mold were 4 cm (Diameter) and 3 cm (Height). It was found that the purity of BN should be greater than 99% to avoid any oxidation that would lead to serious damages to the mold during the preheating phase. The BN mold enabled the glass samples to be annealed overnight, which prevented the glass from becoming stuck within the mold itself. By releasing the heat gradually, the annealing process significantly prevented the glass sample from having a thermal shock. In the annealing phase, the BN mold was placed in the middle of the heating

chamber, and the furnace was programed to its lowest temperature. It took about 8 hours to reduce the temperature gradually from 1400°C to 100°C. The furnace was not capable to go lower than 100°C. So, once it reached 100°C, it was turned off to reach the room temperature. The next day, the glass sample was prepared for polishing and ready to be used.

Two types of glass samples were successfully produced. Table 3.2 shows the characteristics of the produced glass samples.

Composition	Thickness	Diameter	Refractive Index (n)
100 g SiO2	3 cm	4 cm	1.68
80 g SiO2 + 20 g PbO	3 cm	4 cm	1.80

The refractive index (n) for the produced glass samples was measured in our lab by using a 650 nm laser as shown in Figure 3.2. After measuring the incident angle (Φ) and the refracted angle (ϕ) for each glass samples, Snell's law was applied to calculate the refractive index:

$$n_{Glass} = \frac{n_{Air} \times \sin \Phi}{\sin \phi}$$

where n_{Air} equals 1.

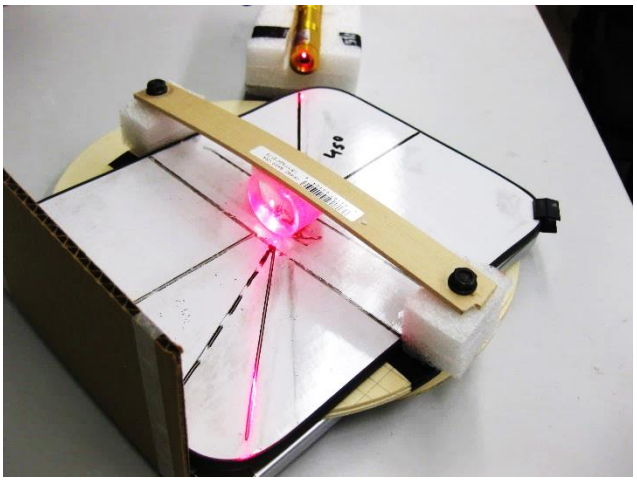

Figure 3. 2 Measuring the refractive index of the glass samples.

3.2 Photomultiplier Tube Setup and Characteristics

A 5.1 cm diameter Hamamatsu PMT model number R2059 was used to characterize the radiation response of the glass samples from a ^{60}Co source. Major properties of the PMT include its high gain 2.0×10^{7}, spectral response ranges from 160 to 650 nm which is well matched with the visible spectrum of Cherenkov light, and a synthetic silica window that is good to transmit Cherenkov light. The synthetic silica has the ability to transmit about 90 % of the visible light down to 200 nm. That percent decreases dramatically as the wavelength becomes shorter toward 160 nm. The PMT was connected to a Nuclear Instrument Modules (NIM) to process the output pulses. The pulses were amplified by a shaping amplifier (CANBERRA 2022), then selected by a Signal Channel Analyzer (SCA) (CANBERRA 2030) and counted by a Timer/Counter unit (CANBERRA 512). The radioisotope source was positioned 3 cm away from the center of each glass sample and along their longitudinal axis. All experiments were occurred using a light tight box. A counting curve was generated by

observing the counts while changing the Hamamatsu R2059 PMT's high voltage to set the appropriate operating bias for the PMT. Figure 3.3 shows the counting curve as a function of the PMT's high voltage. The curve was obtained by placing the PMT inside the dark box without any glass sample. The first part of the curve from -1700 to -1900 V was created by the leakage current. The increase in the counts was linear between -1900 and -2050 V due to the PMT's ability to count single photoelectrons mostly from thermionic emission. When the bias exceeded -2050 V up to -2800 V, the curve represented the field emission and glass or electrode support scintillation [37]. The operation voltage for the PMT was selected to be – 2000 V after the curve of response was analyzed since the output signal could not be more amplified with noise. The chosen bias was fixed for the rest of this work.

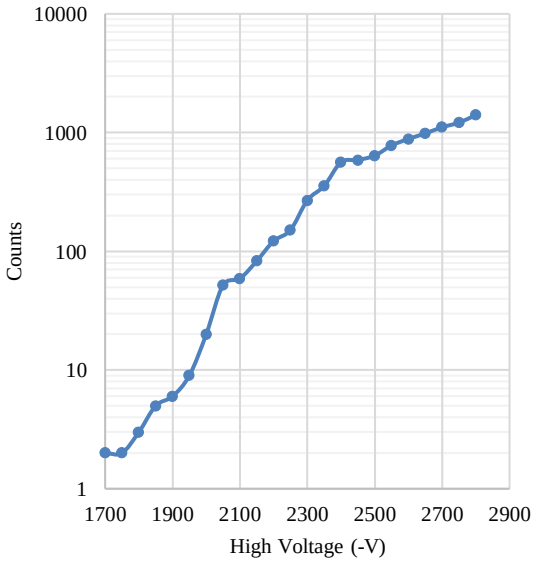

Figure 3. 3 Hamamatsu R2059 PMT counting curve on a logarithmic scale.

The typical spectral response for the used R2059 PMT is shown in Figure 3.4 [38]. It demonstrates Quantum Efficiency (QE) as functions of the wavelengths, the ratio of the number of photoelectrons produced by the photocathode to the number of

incident photons on the photocathode, and is usually expressed as a percentage. The spectral response ranges from 160 to 650 nm which was well matched with the visible spectrum of Cherenkov light. It appears that, the PMT provides maximum response at a wavelength of 420 nm for the QE (27%).

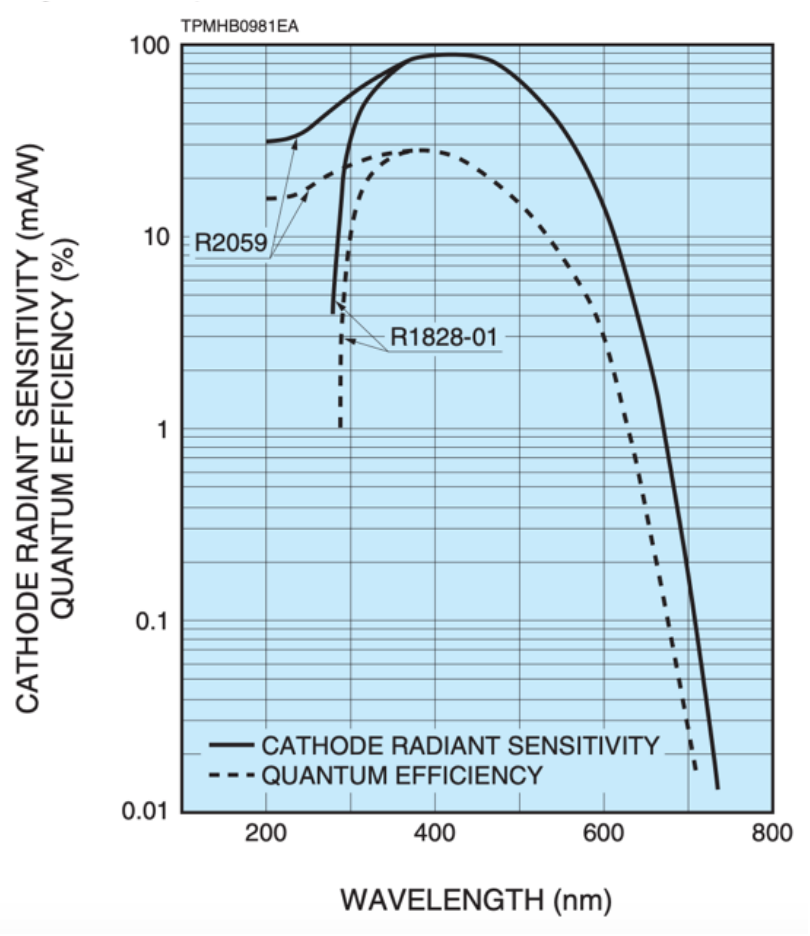

Figure 3. 4 Typical spectral response for R2059 PMT [38].

3.3 Implementation of WLS Fibers

The implementation of WLS fibers was achieved by making a hole inside the glass sample during the melting phase. A 99% purity of BN rod with 6 mm in diameter and 5 cm in length was used. The rod was positioned, held, and inserted inside the molten glass after it was poured into the BN mold by using a specific designed and manufactured stainless steel BN-rods holder (Figure 3.5).

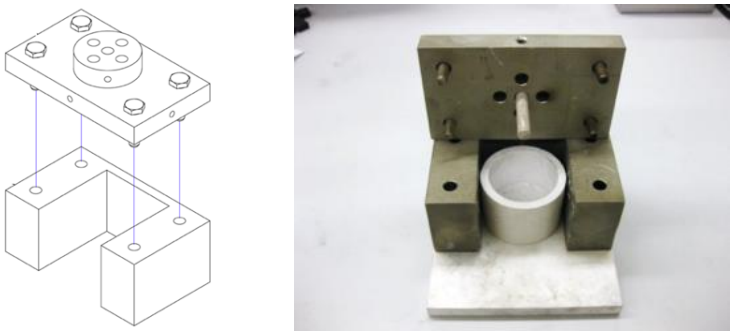

Figure 3. 5 Stainless steel BN-rods holder (left). The picture on the right shows the holder, the BN rod, and the BN mold.

The depth of the hole can be controlled by adjusting the BN rod. The BN mold that contains the molten glass and the rod was left in the furnace overnight to be annealed. After that, the rod was extracted from the hole. Then, the hole was polished, cleaned, and filled with optical grease and 21 WLS fibers (Figure 3.6) since a single fiber has a 1 mm by 1 mm square shape. Although more than one hole can be created in the glass sample, in this proof-of-concept work we focused on producing glass samples with one hole only. Geant4 simulation outputs (Figure 3.7) for the silicon glass sample has shown that the most production of Cherenkov photons occurs at depth 29.5 mm since the range of the energetic electrons in the glass is about 2 mm. To avoid breaking the glass samples, the decision was made to set the depth of the holes to 25 mm.

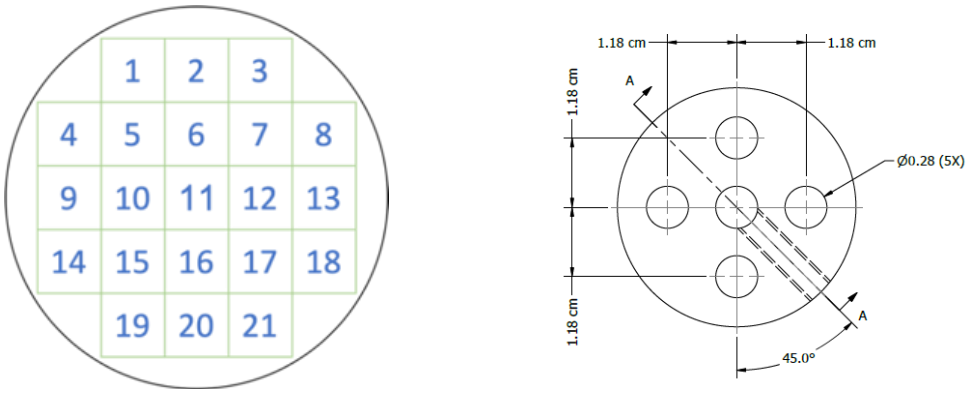

Figure 3. 6 The diagram on the left shows a cross section view inside one hole of a glass sample. It shows 21 WLS fibers. The one on the right shows the configurations of the five holes.

The WLS fibers were made by Saint-Gobain model number BCF-92. The core of it was made of a polystyrene with a refractive index of 1.60 and a density of 1.05 g/cc. In addition to that, a polymethylmethacrylate (PMMA, $C_5H_8O_2$) is a cladding material which has a refractive index of 1.49 and a density of 1.2 g/cc. The WLS fibers absorb Cherenkov photons and emit light with longer wavelengths.

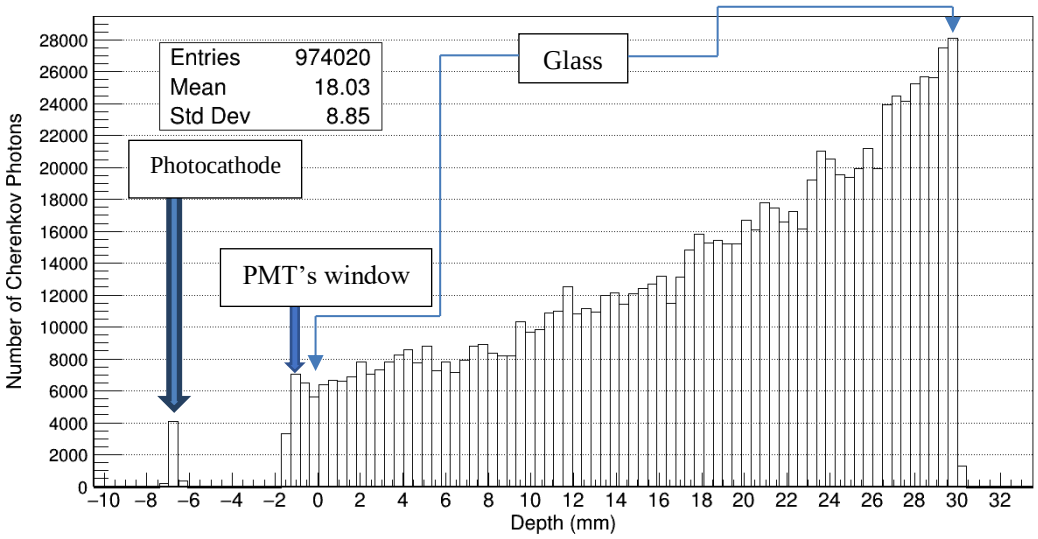

Figure 3. 7 The distribution of Cherenkov photons in the silicon glass by Geant4.

In other words, the fibers absorb photons at a peak of 400 nm and emit them at a peak of 492 nm as shown in Figure 3.8 [39]. The shift process is expected to be helpful when shifting Cherenkov photons because the emission spectrum matches the used PMT.

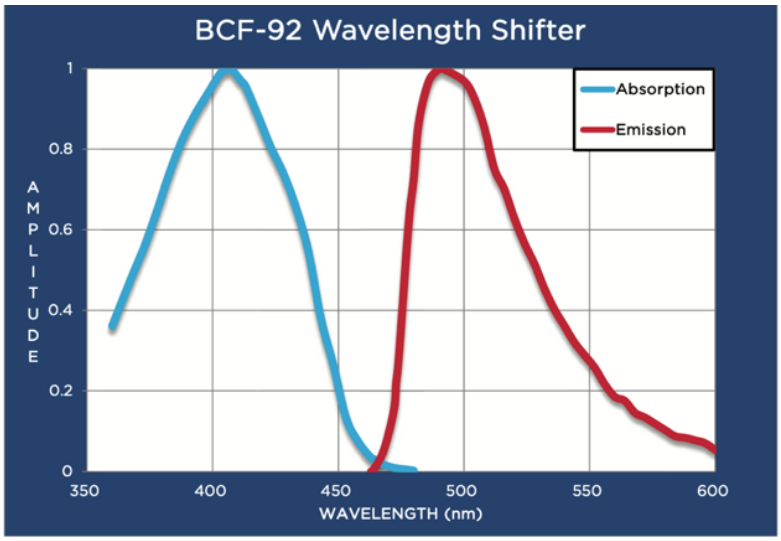

Figure 3. 8 The optical spectra for the used WLS fibers [39].

The used WLS fibers were considered as a fast blue to green shifter with a delay time of 2.7 ns between absorption and re-emission of the new photon. After shifting the wavelength spectrum, the quantum efficiency would reduce accordingly to be 17%. Even though the QE of the PMT is low, the implement of the WLS fibers might be promising to enhance the efficiency and increase the count rate. Without the WLS fibers, the majority of Cherenkov photons are most likely to be absorbed within the glass sample before reaching the photocathode. These fibers cannot directly increase the number of optical photons. However, they can reduce the energy of Cherenkov photons so that they can propagate further in the glass sample and are more likely to create photoelectrons on the photocathode.

3.4 Experimental Setups

For gamma ray measurements, the produced glass samples have been tested by attaching each one to the R2059 PMT and placing them in the dark box along with a 5 µCi ^{60}Co source. An EJ-550 Optical Grade Silicone Grease was applied between the glass sample and the PMT's window. It has refractive index of 1.46 and provides excellent transmission properties into the near-ultraviolet region as shown in Figure 3.9 [40].

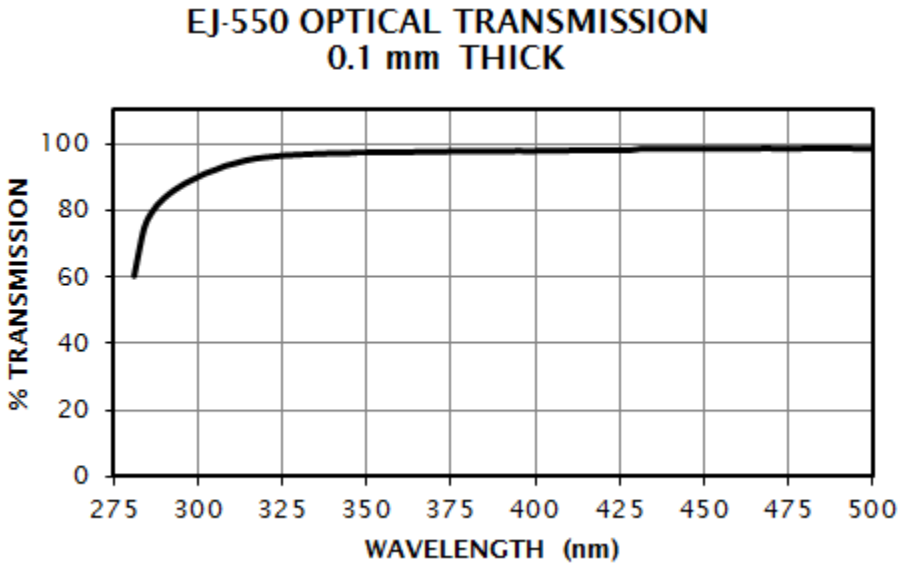

Figure 3. 9 EJ-550 Optical Transmission [40].

The tested glass samples were wrapped by Teflon to reflect most of the optical photons toward the PMT due to its high reflectivity (99%). The distance between the radioactive source and the surface of the detector was 3 cm. The solid angle (Ω) was calculated to be 1.06 based on the source-to-detector distance (d) and the radius of the detector (r) by using the following equation:

$$\Omega = 2\pi\left(1 - \frac{d}{\sqrt{d^2 + r^2}}\right)$$

The decay scheme for ^{60}Co in Figure 3.10 demonstrates the energies emitted and their yields [41]. It decays by β^- emission to excited level of ^{60}Ni. The most important energies from this decay are 1.173 and 1.332 MeV gamma rays since their yields are higher than 99%. These energies are sufficient to interact with the glass samples by photoelectric effect and Compton scattering to produce high energetic electrons. The energies of those electrons should exceed the threshold energy for Cherenkov light to be generated.

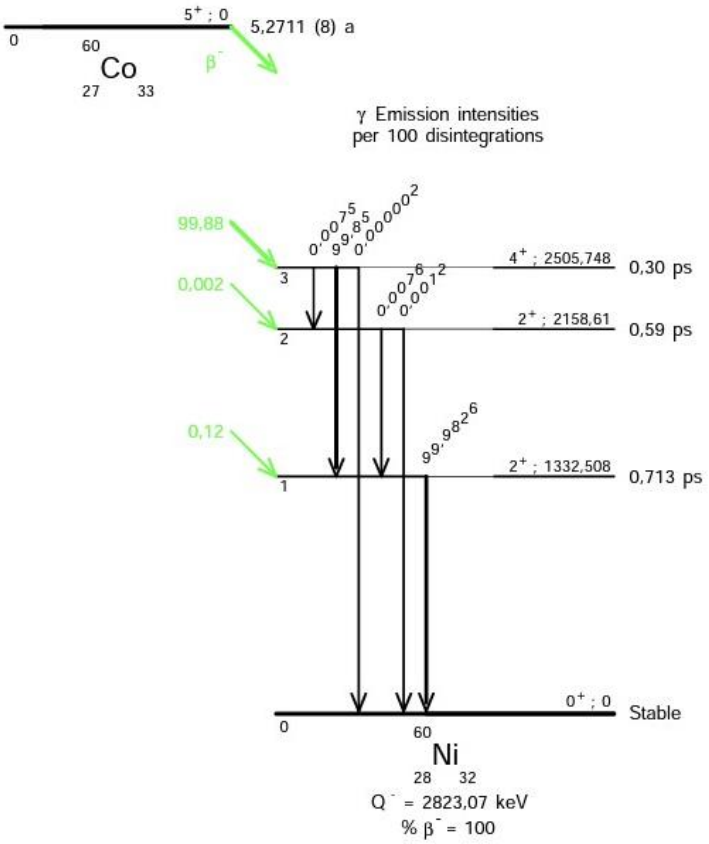

Figure 3. 10 Decay scheme for ^{60}Co [41].

For neutron measurements, the preparation steps of the glass samples were similar to the ones used in the gamma measurements. A PuBe source was used with the activity of 5 Ci, and the neutron yield of the source was 7.91E6 n/sec. The Pu and ^{9}Be were mixed and compressed into a cylindrical shape for encapsulation. The cylinder has dimensions of 3 cm in diameter and a height of 10 cm. The source was placed in a pipe made of steel. The pipe is filled by paraffin and inserted in a container filled by paraffin. Figure 3.11 shows the source configurations.

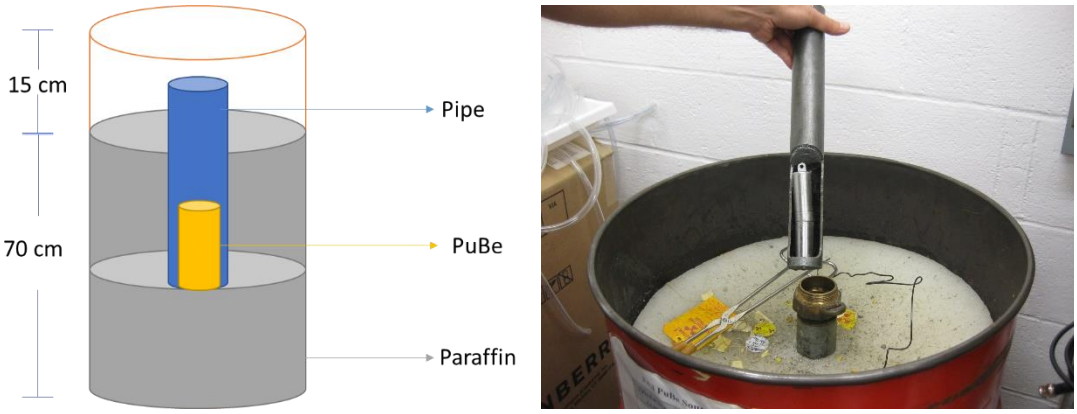

Figure 3. 11 The configuration of the PuBe source.

The detector was placed on the top on the container facing the direction of the neutron beam. A 5 cm lead brick was placed between the container and the detector to attenuate some of the low energy gamma rays coming from the source. The estimated distance between the source and the detector was 29 cm. The estimated neutron flux at measurement position was calculated to be 36 n/cm^{2}sec. The source produces neutrons through the (α,n) reaction. The collision of alpha particles with ^{9}Be produces the following reaction:

$$\alpha + {}^{9}\mathrm{Be} \rightarrow {}^{1}\mathrm{n} + {}^{12}\mathrm{C}$$

The Q-value is 5.71 MeV and is shared among the reaction products. The neutron energy spectrum from PuBe source is shown in Figure 3.12. The excitation state of ^{12}C nucleus causes the several peaks and valleys in this energy distribution [42].

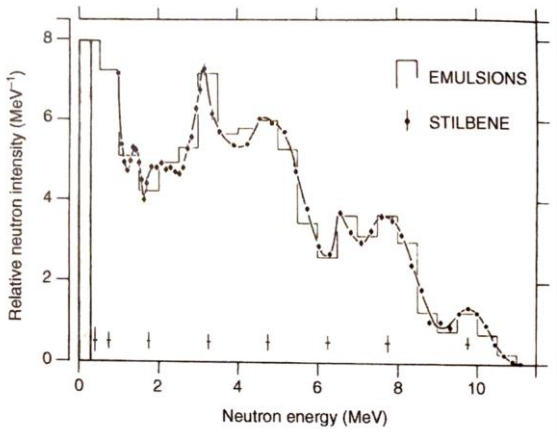

Figure 3. 12 Neutron energy spectrum from PuBe source [42].

In order to detect neutrons from ^{239}PuBe source, Gadolinium Oxide (Gd_2O_3) in powdered shape was used as a neutron activator. Gadolinium is one of the nuclides that has a high thermal neutron capture cross section (254000 b). When a thermal neutron is captured, more than one gamma could be emitted with an average energy of 1.44 MeV [43]. The produced gammas from the neutron capture reaction are expected to interact with the glass samples to generate Cherenkov radiation.

References

[37] Hamamatsu Photonics K. K., “Photomultiplier Tubes Basics and Applications,” 3rd ed., p. 67-68, 2007. Available: https://www.hamamatsu.com/resources/pdf/etd/PMT_handbook_v3aE.pdf (accessed March 11, 2021).

[38] Hamamatsu Photonics K. K., “Photomultiplier Tube R1828-01, R2059,” p.2. Available: https://www.hamamatsu.com/resources/pdf/etd/R1828-01_R2059_TPMH1259E.pdf (accessed March 11, 2021).

[39] Crystals Saint-Gobain, Available: https://www.crystals.saint-gobain.com/sites/imdf.crystals.com/files/documents/fiber-product-sheet.pdf (accessed March 11, 2021).

[40] ELJEN Technology, Available: https://eljentechnology.com/products/accessories/ej-550-ej-552 (accessed March 11, 2021).

[41] Laboratoire National Henri Becquerel, Available: http://www.nucleide.org/DDEP_WG/Nuclides/Co-60_tables.pdf (accessed March 11, 2021).

[42] G. Knoll, “Radiation detection and measurement,” *New York: Wiley*, 3rd edition, p.23, 2000.

[43] T. E. Johnson, B. K. Birky, “Health Physics and Radiological Health,” *Wolters Kluwer*, 4th edition, p 359, 2021.

4 Results and Discussion

This chapter demonstrates the results and the discussion of gamma rays and neutrons measurements for the produced glass samples with and without the WLS fibers while using ^{60}Co and the $^{239}PuBe$ sources. Also, it shows the Geant4 simulation results and the discussion for the Cherenkov glass detectors with several configurations. A detailed explanation about Geant4 simulation and results will be provided in this chapter.

4.1 Gamma Rays Measurement Results

Six glass samples with the same size but different compositions have been produced and tested in our lab. Three of them were made of SiO_2 and the rest were made of $PbO+SiO_2$. Three different configurations were manufactured to observe the effect of WLS fibers on the detection process. Glass A has no holes and no WLS fibers. Glass B and Glass C each had 1 hole and 21 WLS fibers but in different positions. The hole in glass was centered in glass sample C but offset by 1.18 cm in glass sample B. Figure 4.1 shows the three configurations of the glass samples. The same configurations were obtained for silicon and lead glass samples.

Glass A Glass B Glass C

Figure 4. 1 Glass samples produced in our lab with different configurations.

Table 4.1 shows the calculated threshold energies as a result of photoelectric effect and Compton scattering along with the half angle emission for Cherenkov light (θ).

Table 4. 1 Calculated Threshold Energies and the half angle emission for Cherenkov light (θ) for each Sample

Composition	Glass Sample	Half angle emission for Cherenkov light (θ)	Threshold Energy Photoelectric Effect	Threshold Energy Compton Scattering
SiO_2	A	51°	125 keV	252 keV
	B			
	C			
PbO+ SiO_2	A	54°	103 keV	222 keV
	B			
	C			

All the six produced glass samples were tested by attaching each one to the PMT by using EJ-550 optical silicon grease and wrapping each of them by Teflon and placing them in the dark box along with a 5 μCi ^{60}Co source. The PMT's output signals were processed by using the NIM. The distance between the radioactive source and the surface of the detector was 3 cm. Table 4.2 shows a summary of the count rate for the glass samples.

Table 4. 2 Measured count rate for the produced glass samples from ^{60}Co.

Composition	Glass Sample	CPS	Increase
SiO_2	A	22 ± 2	-
	B	73 ± 3	70%
	C	82 ± 3	73%
PbO+ SiO_2	A	84 ± 4	-
	B	141 ± 5	40%
	C	202 ± 6	58%

The count rate (CPS) for each sample was calculated by dividing the net counts by the counting time. The net counts were obtained after subtracting the background count from the gross count. The CPS increased by 73% when WLS fibers were implemented in the center of the silicon glass sample (SiO_2) and reached about 70% when the location of the WLS materials were moved away from the center. The effect of changing the location of WLS fibers on increasing the count rate was about 11%. On the other hand, lead glass sample C showed an increase in count rate by 58% when the WLS fibers were inserted into the center of the glass. However, the count rate was reduced by 30% when the WLS fibers were off the center as in glass B.

The effect of adding lead oxide and the WLS fibers was approached. The count rate was increased by 74% between silicon glass A and lead glass A. This proved that the probability of interactions had increased, and gamma rays interacted more in the lead glass than the silicon glass. Consequently, the number of produced Cherenkov photons was higher in lead sample and propagated the photocathode to generate photoelectrons. Adding the WLS fibers made the Cherenkov detectors more efficient. The count rate increased by 48% between glass B samples and rose by 59% between glass C samples.

Additionally, by knowing the detector's diameter and the distance between the source and the detector, the solid angle (Ω) was calculated and found to be 1.06. Since the radioactive source emits radiation isotopically, only 8.40% of the emitted radiation was incident on the detector. The intrinsic and absolute efficiencies for each glass sample were calculated and the results are shown in Table 4.3. The absolute and intrinsic efficiencies were calculated by:

$$\varepsilon_{\text{Absolute}} = \frac{CPS}{Activity\ (Bq)}$$

$$\varepsilon_{\text{Intrinsic}} = \frac{\varepsilon_{\text{Absolute}} \times 4\pi}{\Omega}$$

Table 4. 3 Calculated efficiency for the glass samples

Composition	Glass Sample	Intrinsic Efficiency	Absolute Efficiency
SiO_2	A	0.137%	0.012%
	B	0.449%	0.038%
	C	0.506%	0.043%
PbO+ SiO_2	A	0.538%	0.045%
	B	0.904%	0.076%
	C	1.294%	0.109%

Implementing the WLS fibers and adding lead oxide increased efficiency by 73% when the lead oxide was added to glass A. Increasing the density of the glass also increased the probability of interaction and count rate. Adding the WLS fibers to glass B in both groups increased the efficiency by 50 %. Also, the C lead glass rose in efficiency 61% more than the C silicon glass.

4.2 Neutrons Measurement Results

The same six glass samples in the gamma measurements were used in the neutron experiments. The neutron source used was a 5 Ci PuBe. These samples were not sensitive to neutrons. Therefore, a neutron activator was used in front of the detector. Gadolinium oxide (Gd_2O_3) was chosen since it has a large capture cross section for thermal neutrons. The effort was made to add Gd_2O_3 to the raw materials of the glass during the molting stage, but it was not a good approach since the gadolinium did not distribute homogenously. Thus, a layer of 1 mm thickness of Gd_2O_3 was used. That thickness was chosen because preparing Gd_2O_3 with thickness less than 1 mm was challenging. Figure 4.2 shows the experiment setup for neutron measurements.

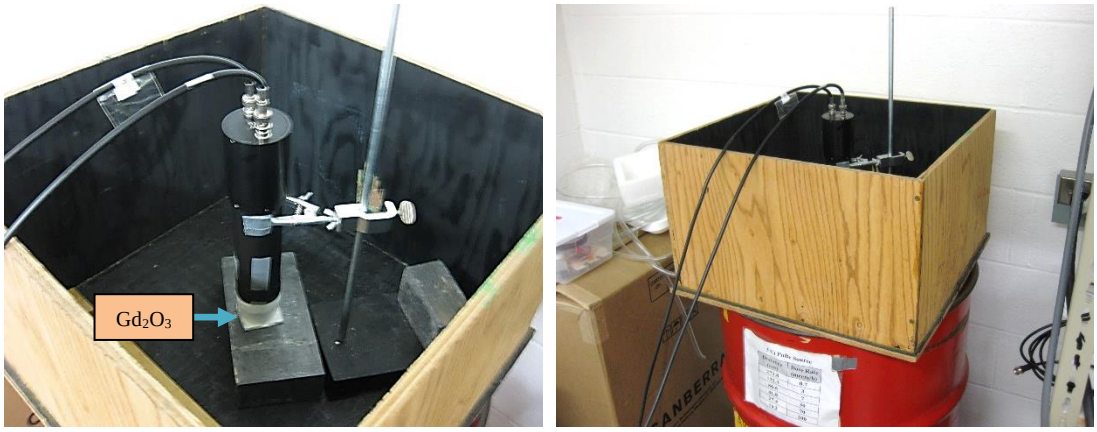

Figure 4. 2 The experiment setup for neutron measurements.

Each glass samples were attached to the PMT and wrapped with Teflon. The detector was held to be facing the PuBe source. The layer of gadolinium was placed between the detector and the lead brick. Since the source was surrounded by Paraffin for shielding purposes, gamma rays released from the container. The detector was exposed to gammas and neutrons at the same time. In order to reduce the number of gammas, a 5 cm thick of lead brick was used to attenuate photons. Increasing the

thickness of lead absorbs the thermal neutrons and prevents them from reaching the activator. The count rate was measured with several thicknesses of lead and the results are shown in Table 4.4.

Table 4. 4 The count rate from ^{239}PuBe source with several lead thickness.

Lead Thickness (cm)	Gd_2O_3 Thickness (mm)	CPS	Increase
0	0	7.03 ± 0.34	20%
	1	8.42 ± 0.37	
5	0	1.05 ± 0.13	33%
	1	1.40 ± 0.15	
10	0	0.68 ± 0.11	25%
	1	0.85 ± 0.12	
15	0	0.48 ± 0.09	10%
	1	0.53 ± 0.09	

The table shows the effect of increasing the lead thickness on the count rate. Without any lead brick, the effect of adding 1 mm of gadolinium on the count rate was 20%. By increasing the lead thickness to 5 cm, the difference between the count rates was 33%. Adding more lead 10 cm and 15 cm had decreased the effect of Gd_2O_3 on the count rate to 25% and 10% respectively. As a result, a thickness of 5 cm lead was selected to be fixed during the measurements.

Table 4.5 shows the results of neutron measurements. The count rate for lead samples were higher than the silicon samples. The effect of adding Gd_2O_3 was observed on both types of glass. Also, the WLS fibers had increased the count rate by more than 115% in the silicon samples and more than 20% in the lead samples. A difference in the count rate was observed after changing the position of the WLS fibers. The count rate had raised up on average by 47% when the fibers were moved from the center of the glass.

Table 4. 5 Count rate measurements for the glass samples from PuBe source.

Composition	Gd_2O_3	Glass Sample	CPS	Increase
SiO_2	0 mm	A	1.05 ± 0.13	-
		B	2.27 ± 0.19	116%
		C	3.42 ± 0.24	226%
	1 mm	A	1.40 ± 0.15	-
		B	3.78 ± 0.25	170%
		C	5.20 ± 0.29	271%
PbO+ SiO_2	0 mm	A	7.47 ± 0.35	-
		B	9.48 ± 0.40	27%
		C	14.65 ± 0.49	96%
	1 mm	A	13.38 ± 0.47	-
		B	16.25 ± 0.52	21%
		C	23.47 ± 0.63	75%

4.3 Geant4 Simulation and Results

Cherenkov glass detectors have been simulated and modeled using Geant4 simulation toolkit due to its capability for advanced optical photon transport simulation, providing Cherenkov physics along with the simulation of particle transport and interactions with matter. This simulation also included an isotopic emission of gamma rays from ^{60}Co, directed neutron beams towards the detector, gamma ray interactions, neutrons interactions, Cherenkov light creation, light transportation, and parameters to create WLS photons. The function of WLS fibers is to absorb Cherenkov photons and re-emit them in new wavelengths. The new emitted photons are WLS photons, as shown in Figure 4.3.

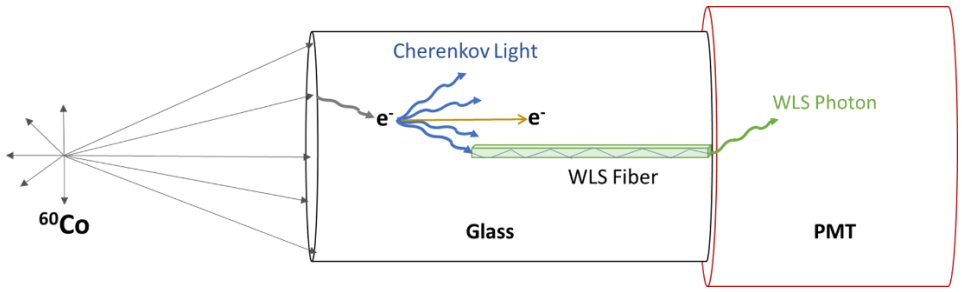

Figure 4. 3 The mechanism of producing WLS photons.

Since the WLS fibers touch the PMT's window, WLS photons emit towards and hit the photocathode. The geometry of the detector was defined in a Text Geometry (TG) file by using a well-defined syntax. In the TG files, the composition of the glass samples, the WLS fibers, the Silicone optical grease, and the neutron activator were defined. A list of predefined materials is provided by Geant4. The compositions of the materials correspond to the National Institute of Standards and Technology (NIST) definition. Two types of glass samples with different compositions have been used, which were SiO2 and SiO2 + PbO. The definition of the two different glass samples is provided below:

SiO_2 Glass:

2 G4_SILICON_DIOXIDE 2.32 139.2 SiO_2

14 1

8 2

:volu Glass TUBE 0 20 15 G4_SILICON_DIOXIDE

SiO_2 + PbO Glass:

:MIXT_BY_NATOMS LeadGlass 6.22 3

Pb 1

Si 1

O 3

:volu Glass TUBE 0 20 15 LeadGlass

The modeling helped to understand and confirm that the measured observations were reasonable. Moreover, Geant4 allows the user to control the surface properties to accurately match material boundaries, as well as to set optical properties of the materials as a function of wavelength. The mechanisms of optical photon are wavelength dependent, and they consist of several parts such as Rayleigh scattering, reflection and refraction inside media and at media boundaries, and photon absorptions. The simulation included the sizes and densities for the glass samples and the PMT's window to demonstrate the optimal configuration for the given application. They emitted energies from ^{60}Co were 1.332 MeV and 1.173 MeV. However, for the ^{239}PuBe source, an energy histogram was provided. Each energy was defined along with their yields of emission. The distance between each source and the detector was set in measurements. In Geant4, Cherenkov photons are generated when a refractive index of a given medium is defined. So, the refractive index for the glass samples, optical grease, and the PMT's window were defined. When gamma rays interact with the detector by photoelectric effect and/or Compton scattering, they produce energetic electrons. Those electrons should exceed the threshold energies to produce Cherenkov light. Cherenkov light may be migrated through the glass sample all the way to the photocathode after passing by the optical grease and PMT window. An approximate thickness of 0.5 mm of silicone grease was modeled between the glass sample and PMT

window. The number of photoelectrons was calculated for each glass samples by multiplying the number of optical photons that reached the photocathode by the Quantum Efficiency (QE) provided by the manufacturer. The QE, generally, is a wavelength dependent and reaches its highest of 27 % for 420 nm. Hamamatsu R2059 PMT with synthetic silica window was used for this modeling. The glass samples were polished and wrapped with a Teflon tape in the experiment in order to allow the Cherenkov photons to be reflected toward the PMT window and was included in the modeling. The reflectivity of the Teflon tape is 99%. Seven configurations have been simulated as shown in Figure 4.4.

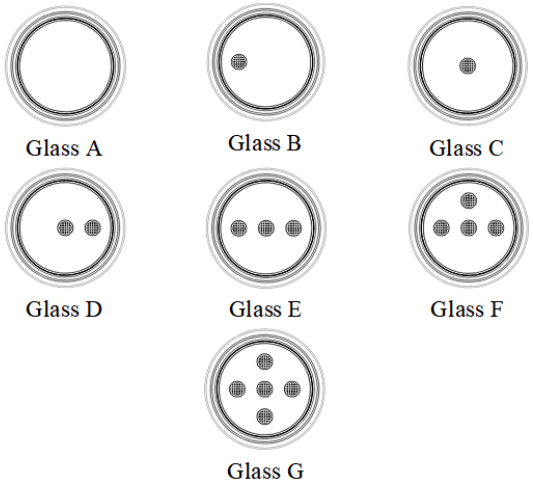

Figure 4. 4 Seven samples with different configurations were simulated by Geant4.

The configurations of glass A, B and C were similar to the ones we produced in our lab, but glass samples D to G were only simulated without being crafted. The following Table 4.6 shows the number of holes and WLS fibers in each glass samples.

Table 4. 6 The number of holes and WLS fibers in each glass samples.

Glass Sample	Number of holes	Number of WLS Fibers
A	0	0
B	1	21
C	1	21
D	2	42
E	3	63
F	4	84
G	5	105

Several parameters needed to be defined in order to simulate WLS fibers, such as a refractive index of the fiber, emission spectrum of the generated photons (WLSCOMPONENT), absorbed lengths of the WLS materials (WLSABSLENGTH), and delay time between the absorption of Cherenkov photon and the re-emission of the new shifted wavelength (WLSTIMECONSTANT). All the parameters were provided by the manufacturer. These parameters are energy dependent and were provided in the TG input files as follows:

:prop Fiber_Core_Polystyrene

*WLSTIMECONSTANT 2.7*ns*

*photon_energies 62 3.451*eV 3.423*eV 3.376*eV 3.331*eV 3.287*eV 3.244*eV*

*3.202*eV 3.161*eV 3.122*eV 3.083*eV 3.068*eV 3.053*eV 3.038*eV 3.023*eV*

*3.008*eV 2.972*eV 2.937*eV 2.903*eV 2.869*eV 2.837*eV 2.804*eV 2.773*eV*

*2.743*eV 2.713*eV 2.683*eV 2.678*eV 2.655*eV 2.632*eV 2.627*eV 2.621*eV*

*2.599*eV 2.588*eV 2.578*eV 2.556*eV 2.535*eV 2.525*eV 2.485*eV 2.465*eV*

*2.446*eV 2.427*eV 2.408*eV 2.389*eV 2.371*eV 2.353*eV 2.335*eV 2.318*eV*

*2.301*eV 2.284*eV 2.267*eV 2.251*eV 2.235*eV 2.219*eV 2.203*eV 2.187*eV*

*2.172*eV 2.157*eV 2.142*eV 2.127*eV 2.113*eV 2.099*eV 2.085*eV 2.071*eV*

//Refractive Index of WLS Fibers

RINDEX 1.60 1.60 1.60 1.60 1.60 1.60 1.60 1.60 1.60 1.60 1.60 1.60 1.60 1.60 1.60 1.60 1.60 1.60 1.60 1.60 1.60 1.60 1.60 1.60 1.60 1.60 1.60 1.60 1.60 1.60 1.60 1.60 1.60 1.60 1.60 1.60 1.60 1.60 1.60 1.60 1.60 1.60 1.60 1.60 1.60 1.60 1.60 1.60 1.60 1.60 1.60 1.60 1.60 1.60 1.60 1.60 1.60 1.60 1.60 1.60 1.60 1.60

// Emission spectrum

WLSCOMPONENT 0.0 0.0 0.0 0.0 0.0 0.0 0.0 0.0 0.0 0.0 0.0 0.0 0.0 0.0 0.0 0.0 0.0 0.0 0.0 0.0 0.0 0.0 0.0 0.0 0.0 0.05 0.52 1.5 2.2 2.8 6.185 7.28 8.66 9.691 9.98 9.98 9.691 9.278 8.557 7.526 7.01 6.289 5.67 5.155 4.536 4.021 3.608 3.196 2.886 2.577 2.165 1.856 1.752 1.459 1.34 1.186 1.031 0.876 0.835 0.773 0.701 0.536

// Absorb Length

*WLSABSLENGTH 0.001*nm 55*cm*

Figure 4.5 shows the emission spectra that were generated by Geant4 for glass samples A to G. The emission of WLS fibers spectra in the figure had a similar shape and peak to the one provided by the manufacturer (see Figure 3. 8 The optical spectra for the used WLS fibers [39].). Most of the WLS photons have wavelengths between

460 to 600 nm. As the number of WLS fibers increase, the number of WLS photons will increase.

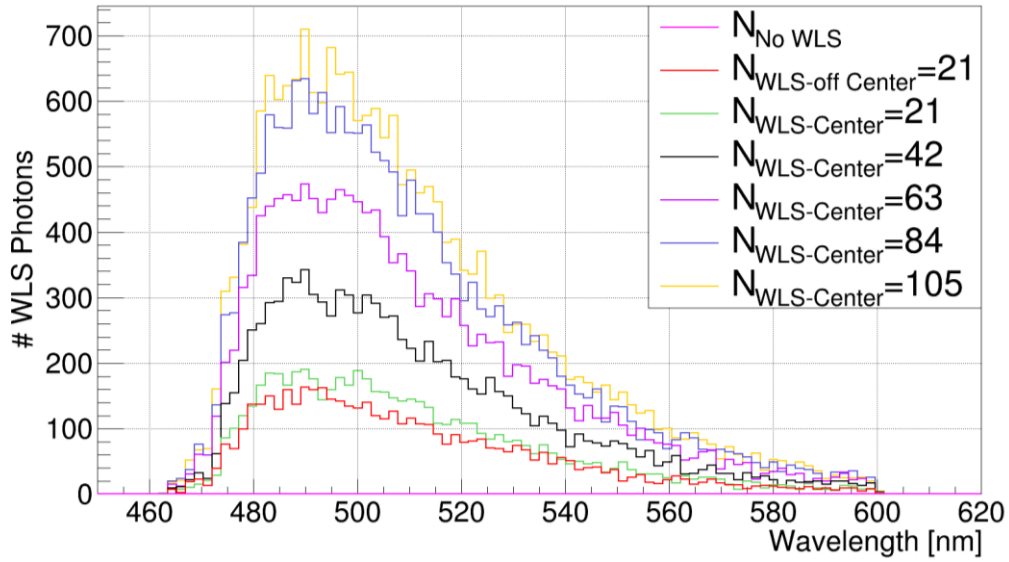

Figure 4. 5 WLS emission spectrum generated by Geant4 for the seven glass samples with ^{60}Co.

It is possible to observe the distribution of the WLS photons to make sure the fibers are in the correct locations and functioning as expected. For example, Figure 4.6 shows an example of a 2D distribution of the generated WLS photons from 105 WLS fibers. The distribution proved the locations of the five holes in the glass sample. Also, the border of each distribution is analogous to the cross-section shape given in Figure 3.8 in chapter 3. WLS photons tended to be mostly generated from the fibers that are located on the edges of the holes. This is reasonable because Cherenkov photons could be absorbed from any point on the fiber, not only from the side that is facing the radioactive source. The absorbed photons had enough energy to reach the core of the fiber and shift its original wavelength to a longer one.

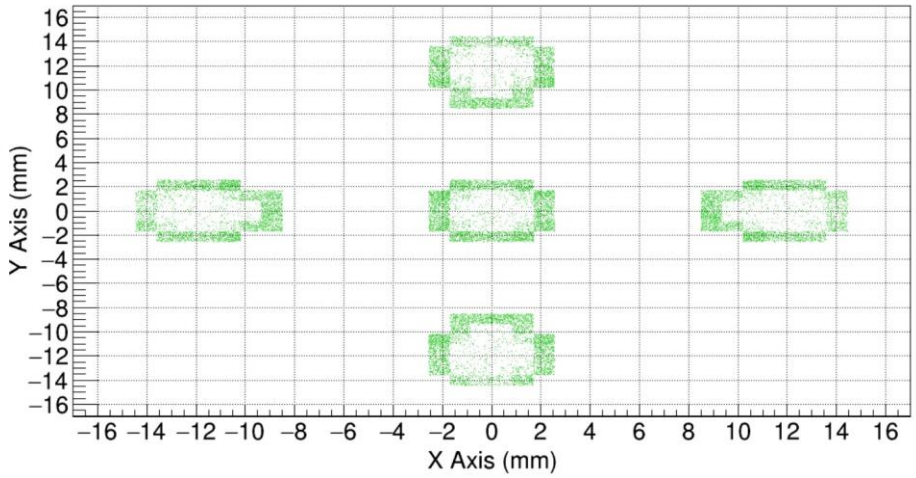

Figure 4. 6 A 2D distribution for WLS photons in glass G.

If the number of WLS photons generated in each hole were compared, we would find the hole in the center generates 10% more photons than each individual outer holes. This percentage matches with the experiment's results.

4.3.1 Geant4 Simulation Results for Gamma Rays

In this part, ^{60}Co has been used as a gamma ray point source, and its activity was 5 µCi. The source emitted gamma rays isotopically. A visualization for the point source and the detector by using HepRApp software is shown in Figure 4.7. The PMT was vacuumed and contained the window and the photocathode. The window was made of a 1 mm of silicon dioxide (SiO_2) and its index of refraction was 1.46. The photocathode was located 5 mm away from the PMT's window and had a thickness of 0.5 mm. The glass sample was attached to the PMT's window. A 5 mm thickness of an optical grease was located between the glass sample and the PMT's window. A 1 mm

of Teflon was added to cover all surfaces of the glass except the one facing the PMT. Also, Teflon was used to cover the remaining area of the PMT's window since the diameter of the window (51mm) was bigger than the diameter of the glass (40 cm). The samples B to G contained holes filled with an optical grease. These holes were the place for the WLS fibers.

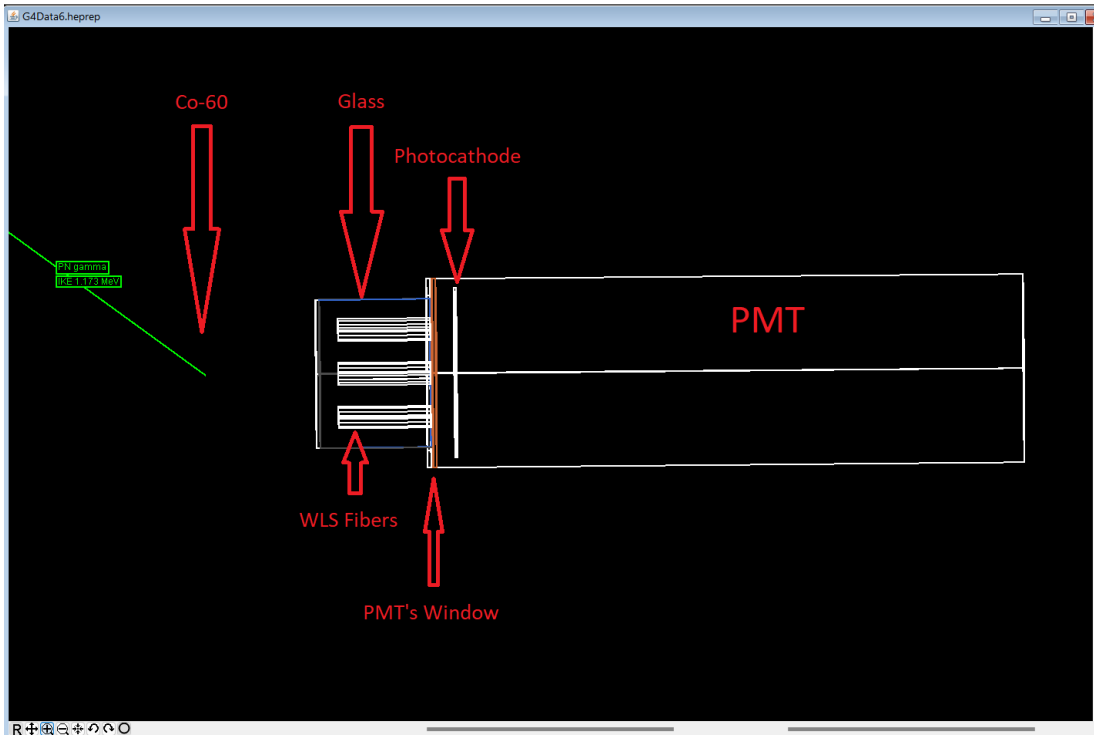

Figure 4. 7 A visualization of the detector and the ^{60}Co source.

The G4GeneralParticleSource (GPS) class and macro commands were used to define the ^{60}Co source. The GPS is part of the Geant4 toolkit for high energy particle transport and allows the user to specify the spectral, spatial and angular distribution of the primary source particles. The following are the macro commands used for defining the ^{60}Co source:

/control/alias pos "0 0 4.6 cm"

/gps/source/set 0

/gps/position {pos}

/gps/ang/minphi 0 deg

/gps/ang/maxphi 360 deg

/gps/source/set 1

/gps/position {pos}

/gps/ang/minphi 0 deg

/gps/ang/maxphi 360 deg

 # Gamma 1

/gps/source/intensity 0.998

/gps/particle gamma

/gps/pos/type Point

/gps/pos/centre {srcpos}

/gps/ang/type iso

/gps/ene/type Mono

/gps/ene/mono 1.173 MeV

 # Gamma 2

/gps/source/add 0.999

/gps/particle gamma

/gps/pos/type Point

/gps/pos/centre {srcpos}

/gps/ang/type iso

/gps/ene/type Mono

/gps/ene/mono 1.332 MeV

The above macro defines the point source centered at (0,0,4.6) cm, which allows the source to be 3 cm away for the surface of the glass by considering the half thickness of the glass (1.5 cm) plus a 0.5 cm thickness of Teflon. The angular distribution is set to be isotopic with a minimum angle of 0 degree to a maximum angle of 360 degrees. The energy distribution is set to be mono-energetic. The energy deposition for gamma rays for the seven configurations with different compositions are shown in Figure 4.8.

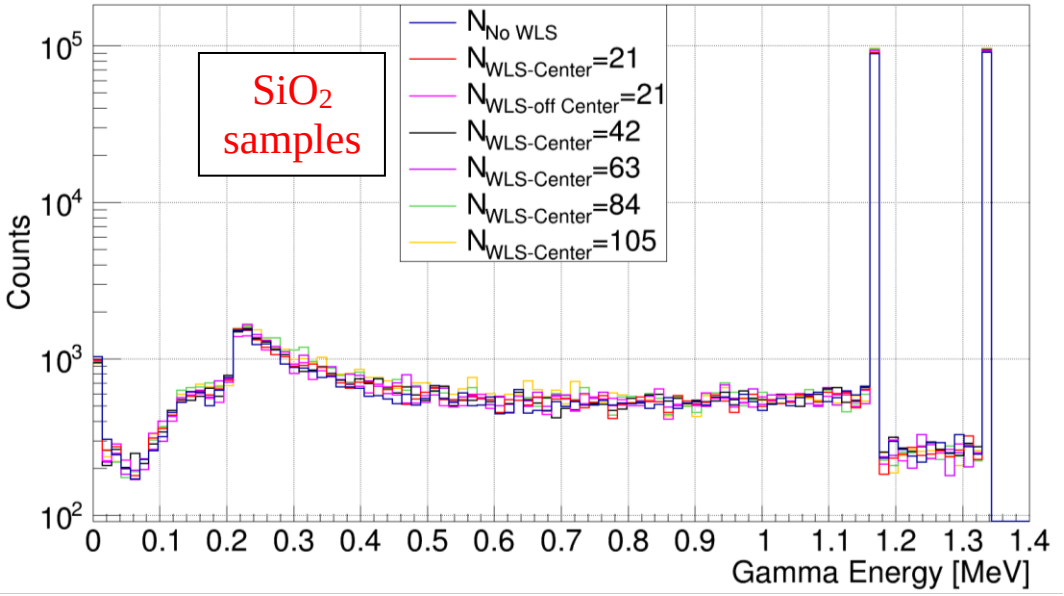

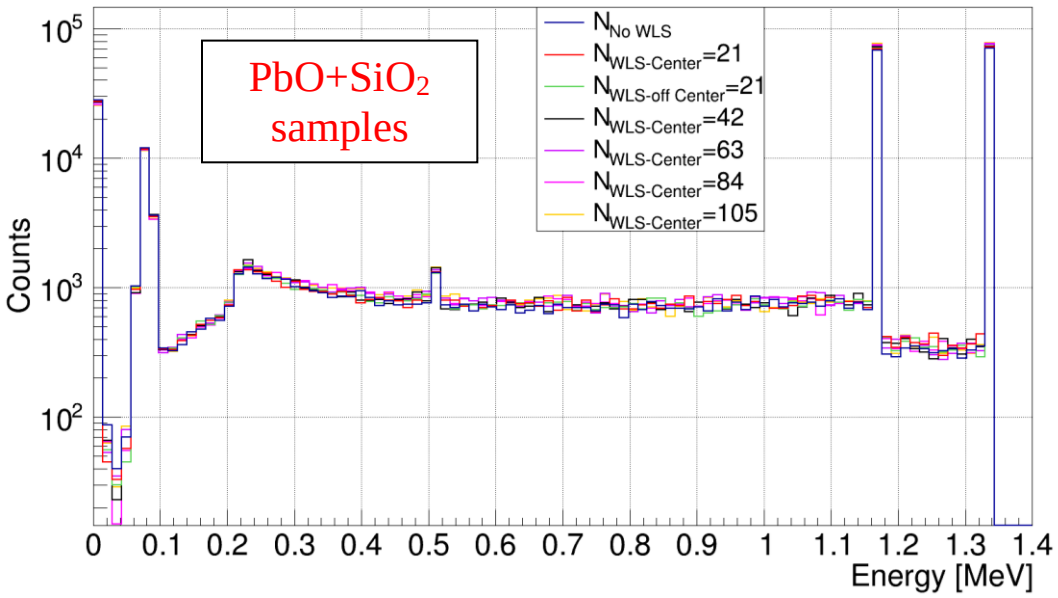

Figure 4. 8 Energy deposition spectra from ^{60}Co with two different glass compositions.

The energy distributions show two remarkable peaks at 1.17 MeV and 1.33 MeV. Also, a backscatter peak is observed at 0.23 MeV due to gamma rays interacting by Compton scattering with the glass. An x-ray peak exists at 70 keV in PbO+SiO_2 glass samples because their Z number is high. The column charts in Figure 4.9 show the number of WLS photons, Cherenkov light, and photoelectrons generate for each simulated samples with different compositions from ^{60}Co.

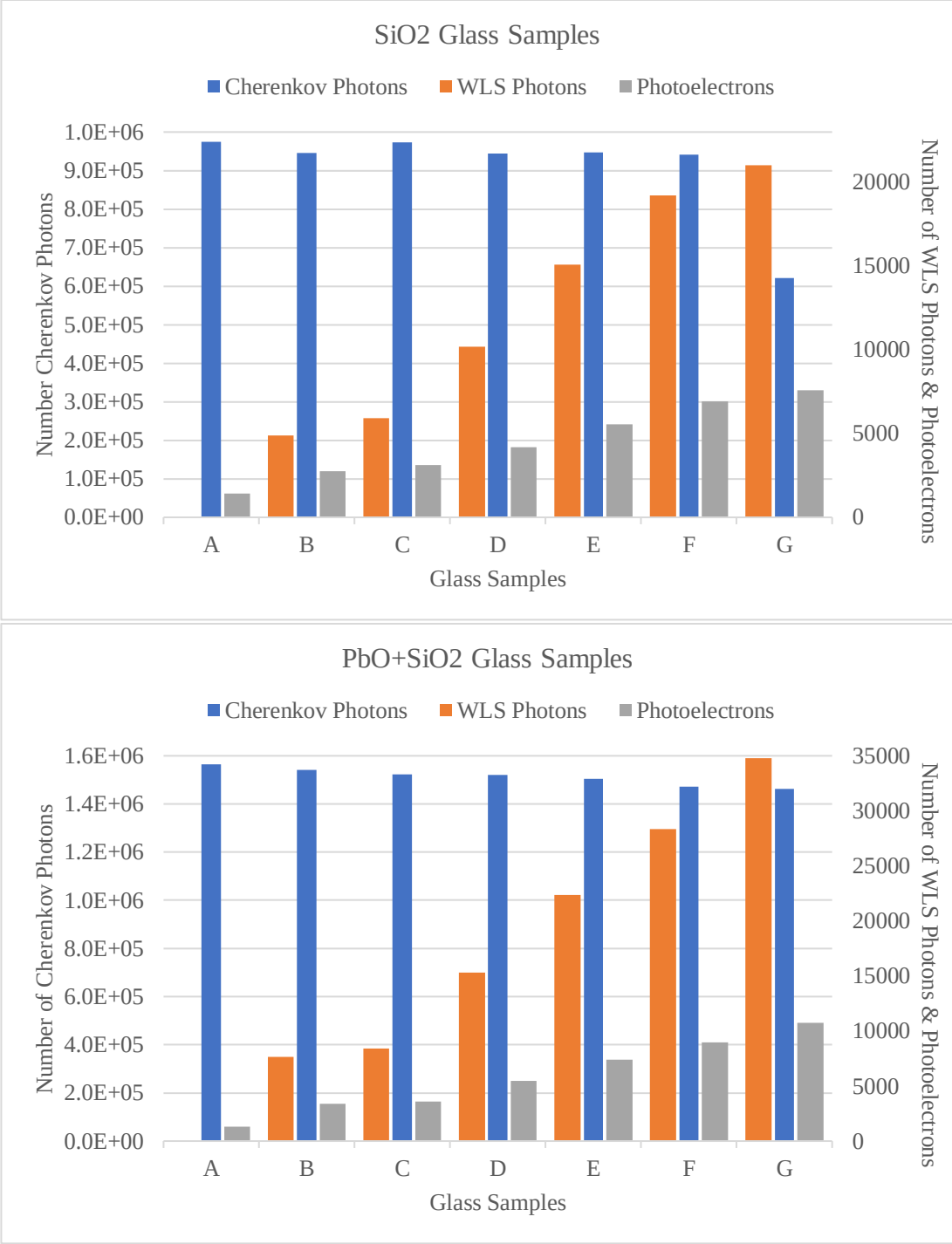

Figure 4. 9 Column chart for the seven simulated samples shows the produced number of Cherenkov photons, WLS photons, and the photoelectrons with two different glass compositions.

In general, the lead samples ($PbO+SiO_2$) showed better output results than the silicon samples (SiO_2). The effect of adding lead oxide to the glass samples had improved the light output. Even though there was not a big difference in the number of produced Cherenkov photons among the samples except for sample G in the silicon group, the effect of WLS materials enhanced the detection efficiency. As the number of WLS fibers increased, the produced WLS photons and photoelectrons increased gradually; however, the generated Cherenkov light decreased. Moreover, the number of photoelectrons increased by 12% between the silicon samples B and C. This rise was expected since the count rate between these two samples increased by 11%. However, the increase in the number of the photoelectrons between B and C in lead samples was about 6%, which was not in agreement with the measurements (30%). Therefore, having WLS fibers implemented in the center of the silicon and lead samples enhanced the produced number of photoelectrons by 54% and 63% respectively.

From the previous charts, a remarkable drop in the number of Cherenkov photons in the SiO_2 glass G was observed. The reduced ratio in the number of Cherenkov light between glass A and G was calculated to be about 36%. This reduction might happen due to parts of the glass sample being replaced with WLS fibers. In other words, the amount of glass was less when the WLS fibers were implemented in glass G. The volume of one hole is 0.71 cm^3, and for five holes are 3.53 cm^3. Glass A has a volume of 37.70 cm^3. This means the volume of the five holes constructs about 10% of glass A. The implementation of the WLS fibers between A and G samples was effective since the number of photoelectrons had increased by 81% for SiO_2 group and 88% for $PbO+SiO_2$ group. The conversion factor for the WLS fiber is one WLS photon out per

photon incident. Thus, the fraction of shifted Cherenkov photons for each sample is shown in Table 4.7.

Table 4. 7 The portion of Cherenkov light gets shifted.

Composition	Glass Sample	# Cherenkov Photons	# WLS Photons	% Get Shifted
SiO_2	B	945004 ± 972	4887 ± 70	0.52%
	C	972608 ± 986	5905 ± 77	0.61%
	D	943808 ± 971	10200 ± 101	1.08%
	E	946854 ± 973	15094 ± 123	1.59%
	F	941336 ± 970	19215 ± 139	2.04%
	G	620889 ± 789	21012 ± 145	3.38%
$PbO+SiO_2$	B	1541397 ± 1242	7664 ± 88	0.50%
	C	1523430 ± 1234	8404 ± 92	0.55%
	D	1519703 ± 1233	15320 ± 124	1.01%
	E	1504978 ± 1227	22372 ± 150	1.49%
	F	1471305 ± 1213	28337 ± 168	1.93%
	G	1462131 ± 1209	34792 ± 187	2.38%

The portion of shifted Cherenkov light increased as the number of the WLS fibers increased. The table shows a consistent increase from B to G samples with different compositions in the amount of Cherenkov light that was converted into WLS photons. As a result of this increase, the optical photons reaching the photocathode increased since the WLS photons increased. Figure 4.10 represents the energy distributions for the optical photons on the photocathode for the silicon and lead samples. A peak at 2.5 eV in both histograms represents the effect of adding WLS fibers to the glass samples. Additionally, adding high z materials like lead oxide to the glass samples enhanced the light output by generating more Cherenkov light and, consequently, producing more WLS photons towards the photocathode.

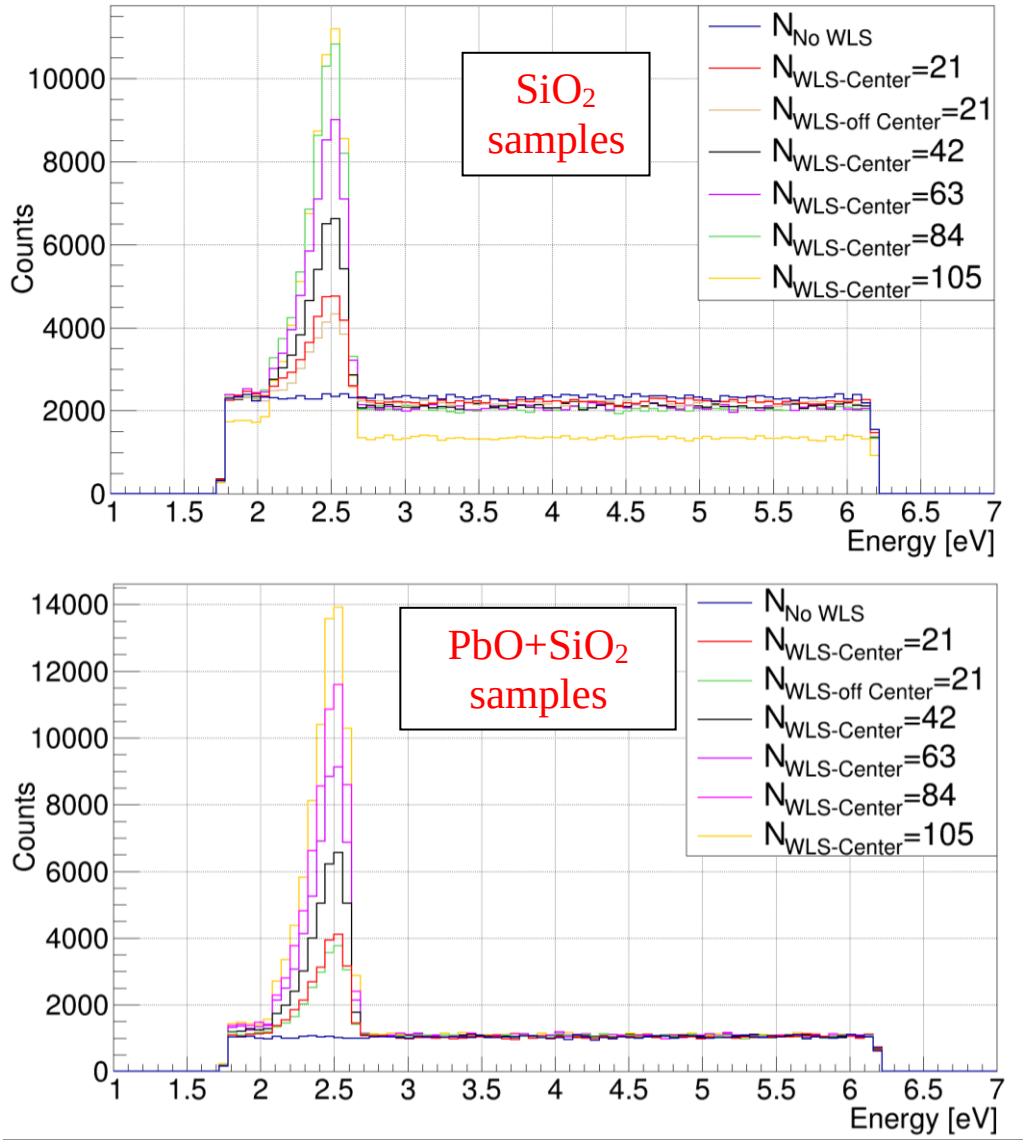

Figure 4. 10 Energy spectra for the optical photons on the photocathode from samples with different compositions.

4.3.2 Geant4 Simulation Results for Neutrons

In this part, ^{239}PuBe source has been used as a neutron source, and its activity was 5 Ci. The source was set to emit neutrons towards the detector only to save time and avoid producing a huge size of output file with unnecessary details. A visualization for the point source and the detector by using HepRApp software is shown in Figure 4.11.

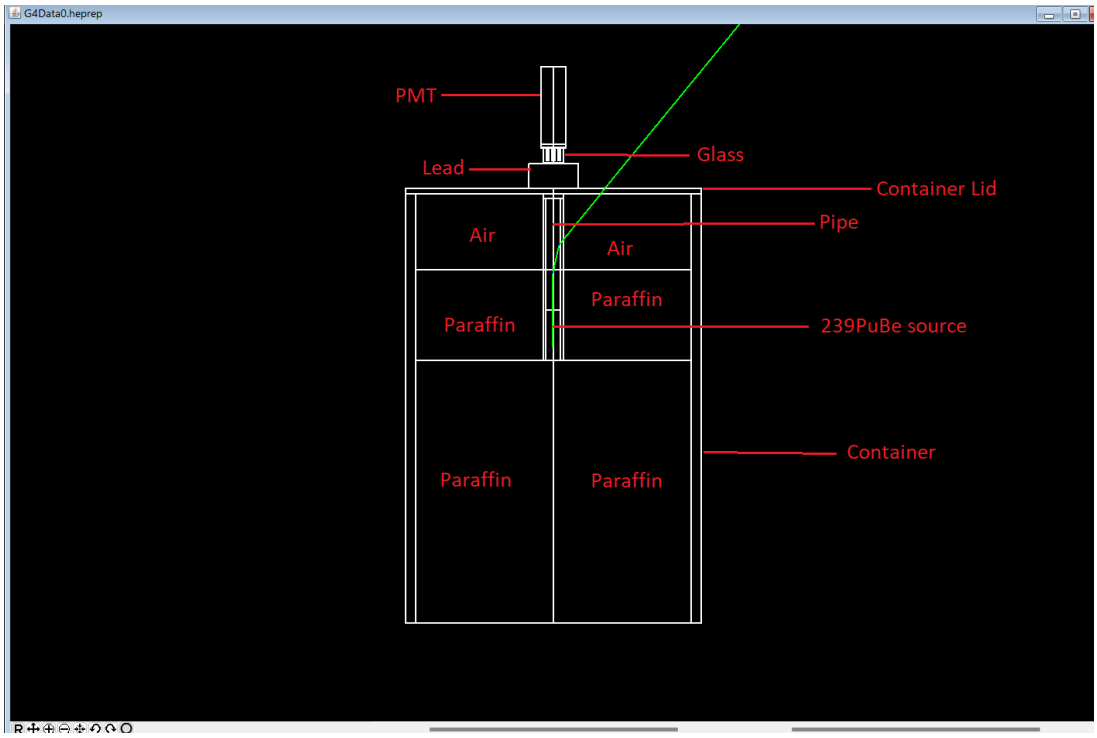

Figure 4. 11 A visualization for the detector and the ^{239}PuBe source.

The modeling of the PMT and the glass was similar to the one used with the gamma rays. Additionally, the ^{239}PuBe source was modeled as accurately as possible. The height of the container was 85 cm, and the thickness of the lid was 1 cm. It had an inner diameter of 56 cm and an outer diameter of 60 cm. The container was filled with a 70 cm thickness of Paraffin, which had an inner diameter of 4 cm and an outer diameter of 56 cm. A pipe made of steel with a height of 33 cm and a diameter of 4 cm was inserted in the Paraffin. The pipe was filled with a 23 cm thickness of Paraffin. The remaining of 10 cm height from the bottom of the pipe was designed to contain the ^{239}PuBe source. A 15 cm air gap was between the Paraffin's surface and the container's lid. On the top of the container's lid, a 5 cm lead brick was placed to attenuate low energy gamma rays coming from the moderated neutrons. Increasing the thickness of the lead would reduce the number of the thermal neutrons reaching the neutron

activator. Two different thicknesses (1 mm and 10 μm) of Gd2O3 were modeled as a neutron activator and were placed between the lead brick and the detector.

Similar to ^{60}Co, the GPS class and macro commands were used to define the ^{239}PuBe source.

 # Neutron Spectrum

/gps/particle neutron

/gps/position 0 0 35.601 cm

/gps/direction 0 0 -1

/gps/ene/type User

/gps/hist/type energy

/gps/pos/type Volume

/gps/pos/shape Cylinder

/gps/pos/radius 1.5 cm

/gps/pos/halfz 5 cm

The above macro defined the neutron source to be at (0,0,35.601) cm, which set the source to be 29.001 cm away for the surface of the detector. A distribution of neutron energies was provided, and each point of energy was specified. Neutrons were to be directed toward the detector. The energy spectrum for neutrons is shown in Figure 4.12. The neutron spectrum shows a peak at about 2 MeV; then the energy decreases gradually. The neutrons were moderated by Paraffin before reaching the detector. In the moderation phase, gamma rays were produced due to the elastic and

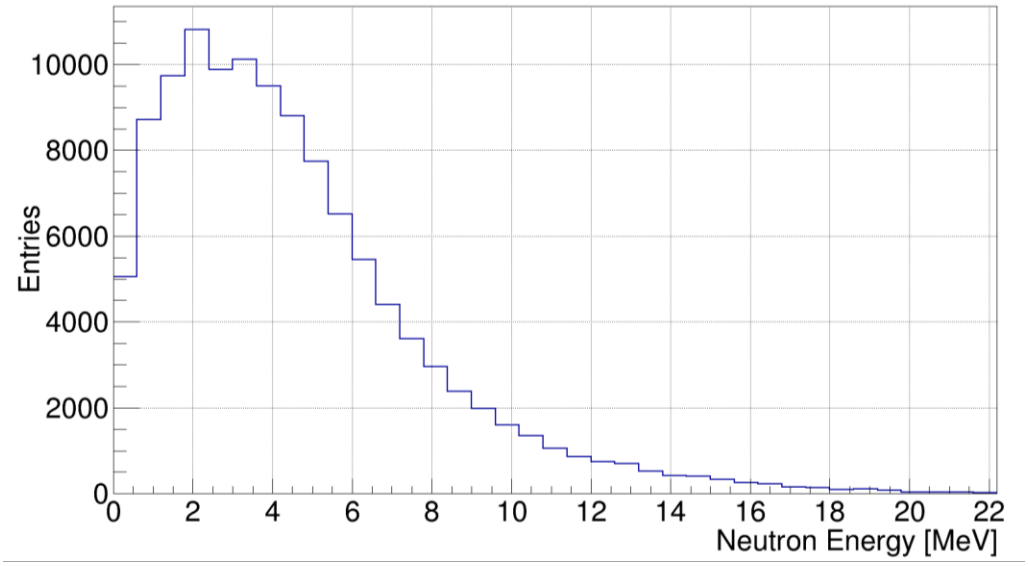

Figure 4. 12 Neutron energy spectrum.

inelastic scattering of the neutrons. Also, the absorption of thermal neutrons by the surrounding materials such as Paraffin, steel, and lead produced gamma rays. Having the lead brick between the container and the detector could attenuate some of the gamma rays but not all of them. So, the detector was exposed to neutrons and gamma rays. The focus was to distinguish between them and test the samples with neutrons. Thus, the glass samples were simulated with and without Gd_2O_3. The activator was placed in front of the detector. The absorption of the thermal neutrons by gadolinium releases high energy gamma rays. These gammas could interact with the glass to produce Cherenkov light. Figure 4.13 shows the Cherenkov spectra for different configurations, glass compositions and several thicknesses of Gd_2O_3.

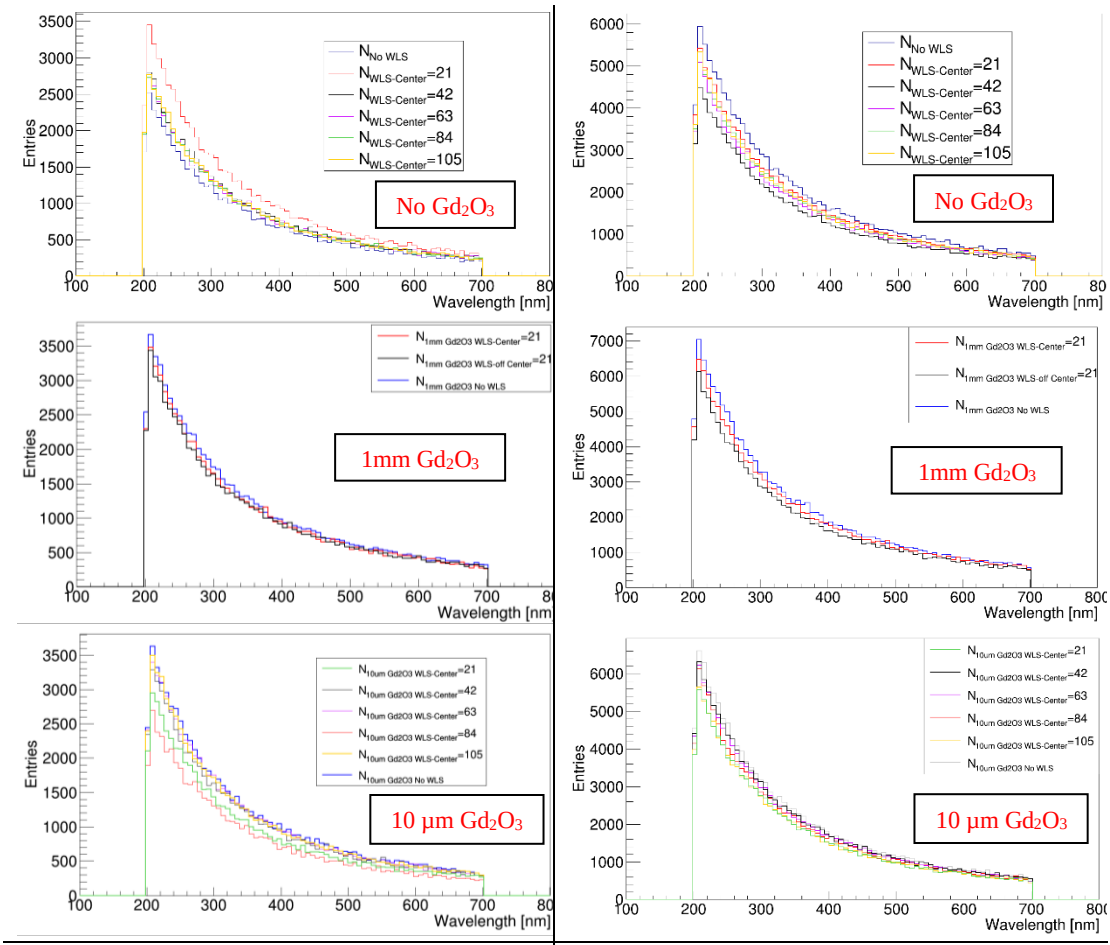

SiO_2 glass samples	$PbO+SiO_2$ glass samples

Figure 4. 13 Cherenkov spectra for different configurations, glass compositions and several thicknesses of Gd_2O_3.

The previous figure represents six graphs for Cherenkov light produced in different composition of glass samples, with different number of WLS fibers and several thicknesses of Gd_2O_3. The lead samples produced more Cherenkov photons than the silicon samples. Most of the samples with no WLS fibers generated more Cherenkov light than the others. 1 mm of gadolinium oxide was modeled with glass samples of 21 WLS fibers to evaluate the measurement results. Since preparing Gd_2O_3 with thickness less than 1 mm was challenging, 10 µm thickness was only simulated to observe the difference of changing the thickness. Having a thicker layer of gadolinium

will capture more thermal neutrons; however, the produced gammas may not be emitted towards the detector. Figure 4.14 shows the gamma rays released as a result of neutron capture in 1 mm and 10 µm thickness of Gd_2O_3.

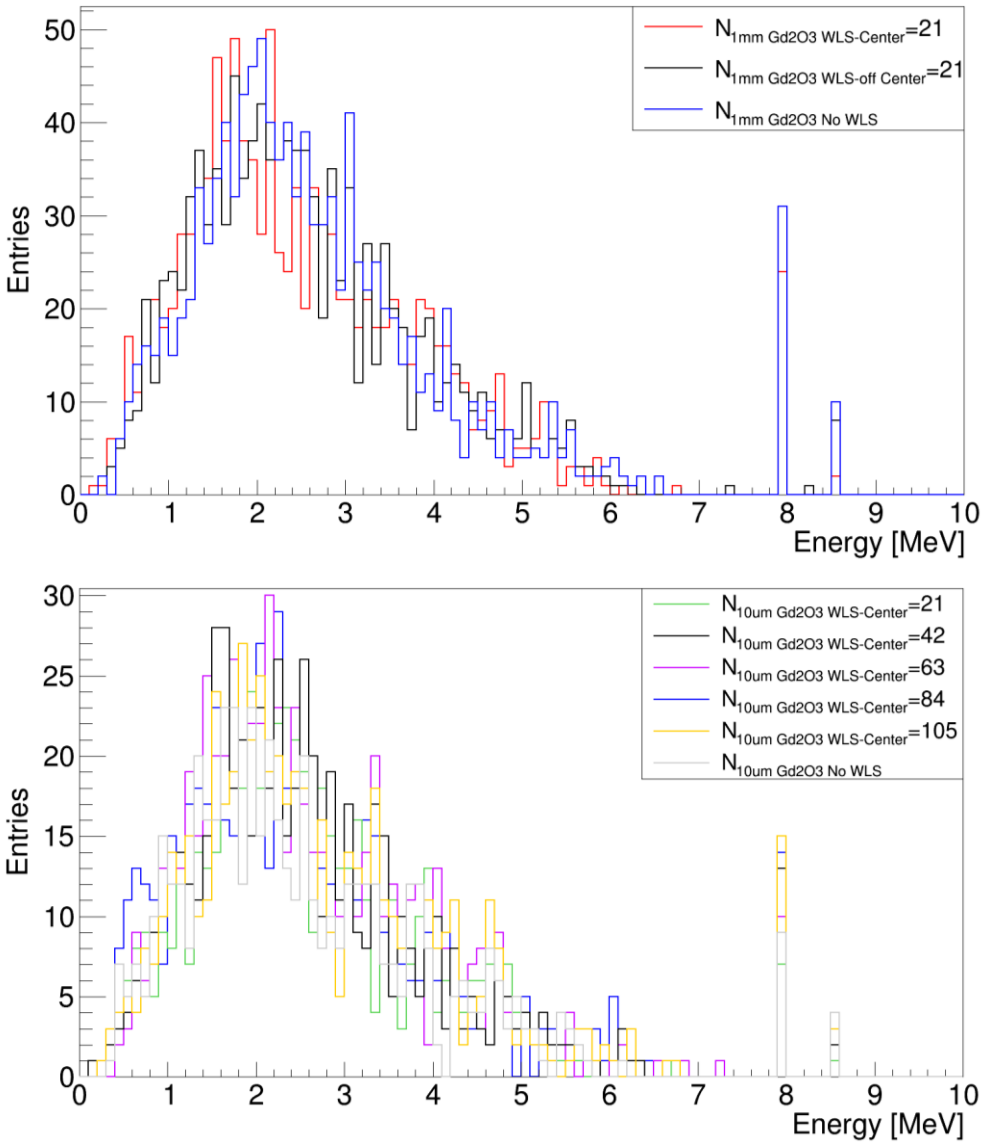

Figure 4. 14 Gamma rays released from neutron capture in 1 mm and 10 µm of Gd_2O_3.

The two graphs were chosen for the lead samples. Similar graphs with similar output were obtained for the silicon samples but not shown here. Gamma rays were produced more with 1 mm of gadolinium than the thinner one. Two peaks at 8 and 8.6

MeV appeared on both histograms. They were released for the reactions of Gd (n,γ). Figure 4.15 displays the gamma spectrum in the glass samples.

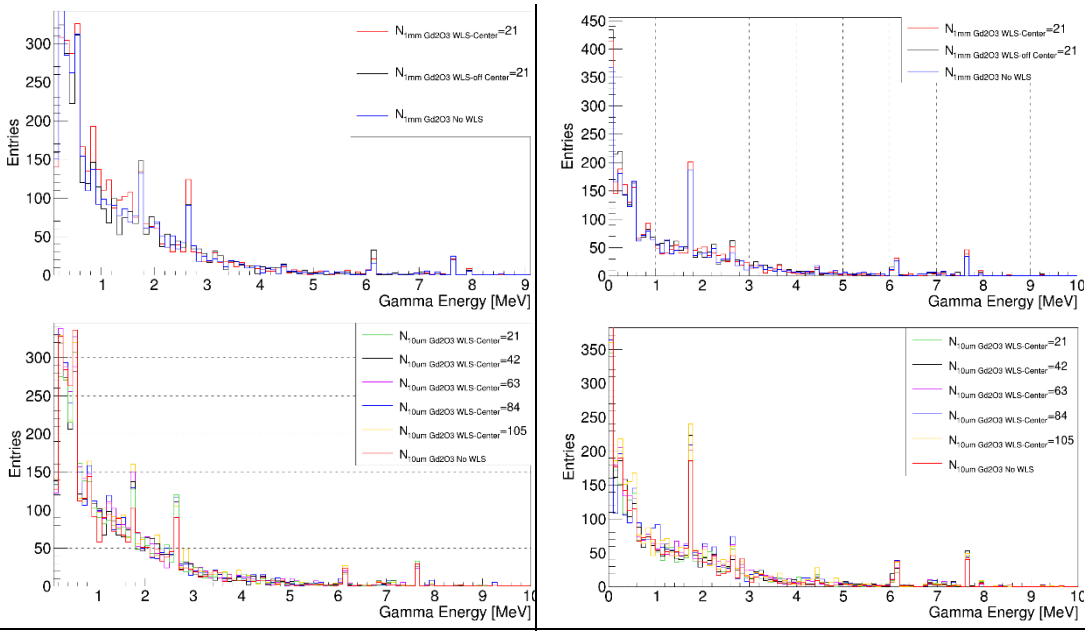

PbO+SiO_2 glass samples | SiO_2 glass samples

Figure 4. 15 Gamma spectra in the glass samples.

Several peaks can be observed from the graphs such as 1.7 and 7.6 MeV. A few of the gammas from the neutron capture interactions in gadolinium reached the glass samples. The interactions of the gammas with the glass samples produced Cherenkov photons. As a result of these interactions, the energy distributions for the optical photons on the photocathode for the silicon and lead samples with different thickness of Gd_2O_3 are shown in Figure 4.16. It was expected the observe the WLS photon peaks, proving that the fibers were functioning appropriately. The light output increased when adding WLS fibers to the glass and lead oxide. Even though there were not so many gammas released from the neutron captured in gadolinium, the effects of adding lead oxide to samples was observed.

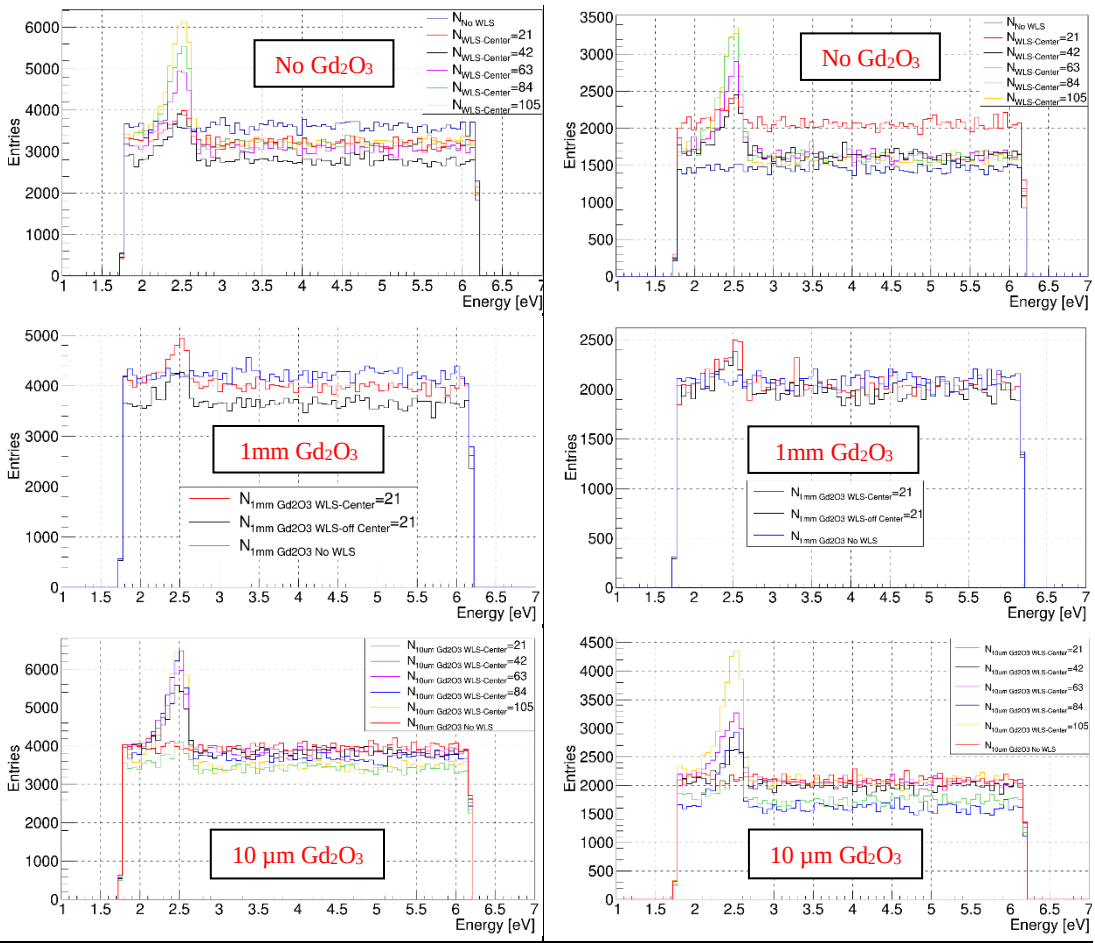

PbO+SiO_2 glass samples	SiO_2 glass samples

Figure 4. 16 Energy spectra for the optical photons on the photocathode with samples with different compositions and different thickness of Gd_2O_3.

5 Conclusion

In this work, the effect of WLS fibers on increasing the detection efficiency for Cherenkov glass detectors has been studied. Also, a Geant4 simulation toolkit was used to build a detailed model and to understand and confirm that the measured observations were reasonable. The approach was to improve the light output of Cherenkov detectors and make them more efficient by adding lead oxide to the glass and incorporating the WLS fibers. The purpose of having lead oxide in the raw materials of the glass samples was to increase the probability of interaction between the incident gamma rays and the detector. The WLS fibers have the ability to shift the spectrum of the Cherenkov radiation towards longer wavelength, reduce the number of Cherenkov photons absorbed by the glass, and improve coupling with the photomultiplier Tube.

Six produced glass samples with different compositions and configurations were examined. Three silicon (SiO_2) and three lead ($PbO+SiO_2$) glass samples were produced. Each group had the similar configurations by making Cherenkov glass samples with and without the WLS fibers. Glass A had no WLS materials, but glass B and C contained WLS fiber in various locations. A hole of 25 mm in depth and 6 mm in diameter was created in samples B and C to make a place for the implementation of 21 wavelength shifters. The hole in the glass was centered in glass sample C but offset by 1.18 cm in glass sample B. Generally, the light output was higher with the lead samples than the silicon samples. This was expected since the Z number of the lead samples were higher than the silicon samples. Also, the count rate had increased in the presence of WLS fibers and was slightly higher in glass C than glass B when the samples were exposing to ^{60}Co and $^{239}PuBe$ sources. Gamma ray measurements

showed that the count rate was increased by 70% in the silicon glass B and 73% in the silicon sample C. Adding lead oxide to samples B and C increased the count rate by 40% and 58% respectively. In the neutron measurements, 1 mm of Gd_2O_3 was used to capture thermal neutrons since gadolinium has a large cross section for capturing thermal neutrons. The layer of gadolinium was positioned in front of the detector to allow the released gammas to interact with the glass sample. The measurement results showed the effect of adding lead oxide and the WLS fibers to the samples.

Seven configurations were simulated by Geant4 toolkit with gamma rays and neutrons. The result showed the number of WLS photons and photoelectrons were increasing as the number of fibers increased. Even though glass G produced the greatest number of WLS photons and photoelectrons, it generated the smallest amount of Cherenkov light. This proved the WLS fibers were functioning by absorbing part of the Cherenkov light into WLS photons. The lead glass samples showed an increase in the light output compared to the silicon glass samples even though the released gamma rays from neutron capture in gadolinium was not enough to make a huge difference in the light output.

Bibliography

A. Anatoli, M. A. Billercia, “Scintillation-Cherenkov detector and method for high energy X-ray cargo container imaging and industrial radiography,” US Patent US 2011/0163236 A1, 2011.

B. Ayaz-Maierhafer, et al., “Investigation of active background from photofission in depleted uranium using Cherenkov detectors and gamma ray time-of-flight analysis,” *IEEE Trans Nucl Sci* 61:2402–2409, 2014.

B. Ayaz-Maierhafer, et al., “Measurement of thermal neutron response in Cherenkov glasses designed for MeV photon detection,” *IEEE Trans Nucl Sci* 60:701–707, 2013.

B. Ayaz-Maierhafer, et al., “Sensing of ^{252}Cf fission gamma rays using same-size glass detectors,” *J Radioanal Nucl Chem.,* Vol. 308, p. 919–926, November 2015.

B. Ayaz-Maierhafer, M. Laubach and J. Hayward, "Sensing of ^{252}Cf fission gamma rays using same-size glass detectors," *Journal of Radioanalytical and Nuclear Chemistry,* vol. 308, no. 3, pp. 919-926, 2015.

Crystals Saint-Gobain, Available: https://www.crystals.saint-gobain.com/sites/imdf.crystals.com/files/documents/fiber-product-sheet.pdf (accessed March 11, 2021).

D. Hampf, M. Tluczykont, D. Horns, “Event reconstruction techniques for the wide-angle air Cherenkov detector HiSCORE,” *Nucl Instum Methods* A 712:137–146, 2013.

ELJEN Technology, Available: https://eljentechnology.com/products/accessories/ej-550-ej-552 (accessed March 11, 2021).

Erickson A S., “Remote Detection of Fissile Material: Cherenkov Counters for Gamma Detection,” Ph.D. dissertation, Massachusetts Institute of Technology, 2011.

F. Kocak, I. Tapan, “$PbWO_4$ Cherenkov light contribution to Hamamatsu S81148 and zinc sulfide-silicon avalanche photodiodes signals,” *Nucl Instrum Methods* A 617:398–399, 2010.

G. G. Pang, J. A. Rowlands, “Cherenkov X-ray detector for portal imaging,” US Patent US7297914 B2, 2007.

G. Knoll, “Radiation detection and measurement,” *New York: Wiley*, 3rd edition, p.713, 2000.

G. Knoll, “Radiation detection and measurement,” *New York: Wiley*, 3rd edition, p.23, 2000.

H. R. Vega-Carrillo, et al., “Neutron and gamma-ray spectra of ^{239}PuBe and ^{241}AmBe,” *Applied Radiation and Isotopes*, vol. 57, pp. 167-170, 2002.

H. W. Button-Shafer Churchill, R. L. Lichti, D. H. Novack, “Development of a large low-mass, water Cherenkov counter,” *Nucl Instrum Methods* 137:29–40, 1976.

Hamamatsu Photonics K. K., “Photomultiplier Tube R1828-01, R2059,” p.2. Available: https://www.hamamatsu.com/resources/pdf/etd/R1828-01_R2059_TPMH1259E.pdf (accessed March 11, 2021).

Hamamatsu Photonics K. K., “Photomultiplier Tubes Basics and Applications,” 3rd ed., p. 67-68, 2007. Available: https://www.hamamatsu.com/resources/pdf/etd/PMT_handbook_v3aE.pdf (accessed March 11, 2021).

I. Iijima, et al., “Studies of a proximity focusing aerogel RICH for future Belle upgrade,” *Nucl. Inst. Meth.* A 595:92–95, 2008.

J. Hayward et al., "Characterizing the radiation response of Cherenkov glass detectors with isotopic sources", *Journal of Radioanalytical and Nuclear Chemistry*, vol. 295, no. 2, pp. 1143-1151, 2012. Available: 10.1007/s10967-012-1898-4.

J. P. Hayward, et al., “Characterization the radiation response of Cherenkov glass detectors with isotopic sources,” *J Radioanal Nucl Chem* 295:1143–1151, 2013.

J. P. Hayward, et al., “Simulated response of Cherenkov glass detectors to MeV photons,” *J Radioanal Nucl Chem* 295:1321–1329, 2013.

Laboratoire National Henri Becquerel, Available: http://www.nucleide.org/DDEP_WG/Nuclides/Co-60_tables.pdf (accessed March 11, 2021).

M. Iodice, et al., “The CO2 gas Cherenkov detectors for the Jefferson Lab Hall—a spectrometer,” *Nucl Instrum Methods* A 411:223–237, 1998.

M. Kobayashi, et al., “A beam of PbWO4 Cherenkov radiators,” *Nucl Instrum Methods* A 484:140–148, 2002.

M. Kobayashi, S. Sugimoto, U. Usuki, “Radiation hardness of PbWO4 Cherenkov radiators heavily doped with trivalent rare-earth ions,” *Nucl Instrum Methods* A 524:385–389, 2004.

M. Sweany, A. Bernstein, N. Bowden, S. Dazeley, R. Svoboda, “Special nuclear detection with water Cherenkov based detectors,” *IEEE NSS Conf. Record*, N61-5:3372-3375. Dresden, Germany, 2008.

N. Akchurin, et al., “Contribution of Cherenkoc light to the signals from lead tungstate crystals,” *Nucl Instrum Methods* A 582:474–483, 2007.

P (ed). Carlson “Cherenkov detectors and their applications in science and technology,” *Nucl. Instrum. Methods* A 248, 1986.

P. A. Cherenkov, “Visible light from clear liquids under the action of gamma radiation,” Dokl Akad Nauk SSSR 2:451, 1934.

P. Cenci, et al., “The ring imaging Cherenkov detector of the NA62 experiment at CERN,” *Nucl Instrum Methods* A 732:342–345, 2013.

P. D. Grannis, D. Jaffe, M. D. Marx, “Low-cost glass Cherenkov detectors,” *Nucl Instum Methods* 188:239–242, 1981.

P. Lecoq, et al., “Factors influencing time resolution of scintillators and ways to improve them,” *IEEE Trans Nucl Sci* 57:2411–2416, 2010.

R. Pestotnik, S. Korpar, P. Krizan, R. Dolenec, “Cherenkov detector of 90Sr on aerogel as radiator,” *Nucl Instrum Methods* A 595:278–280, 2008.

S. Dazeley, M. Sweany, A. Bernstein, “SNM detection with an optimized Cherenkov neutron detector,” *Nucl Instrum Methods* A 693:148–153, 2012.

S. I. Vavilov “On possible causes of dark blue radiation in liquids,” Dokl Akad Nauk SSSR 2:457, 1934.

S. Korpar, R. Dolenec, P. Krizan, R. Pestotnik, A. Stanovnik, “Study of TOF PET using Cherenkov light,” *Nucl Instrum Methods* A 654:532–538, 2011.

S. Nishida, et al., “Development of a 144-channel Hybrid Avalanche Photo-detector for Belle II ring-imaging Cherenkov counter with aerogel radiator,” *Nucl Instrum Methods* A 787:59–63, 2015.

T. E. Johnson, B. K. Birky, “Health Physics and Radiological Health,” *Wolters Kluwer*, 4th edition, p 359, 2021.T. Iijima, et al., “Studies of a proximity focusing RICH with aerogel radiator for future Belle upgrade,” *Nucl Instrum Methods* A 595:92–95, 2008.

X. Zhang, J. P. Hayward, M. A. Laubach, “New method to remove the electronic noise for absolutely calibrating low gain photomultiplier tubes with a higher precision,” *Nucl Instrum Methods* A 755:32–37, 2014.

Y. Miyazaki, et al., “Performance test of lead-glass counter for the J-PARC E36 experiment,” *Nucl Instrum Methods* A 779:13–17, 2015.

Z. W. Bell, and L. A. Boatner, “Neutron Detection via the Cherenkov Effect,” *IEEE TNS*, Vol. 57, NO. 6, p. 3800-3806, 2010.

Z. W. Bell, L. A. Boatner “Neutron detection via the Cherenkov effect,” *IEEE Trans Nucl Sci* 57:3800–3806, 2010.

Appendices

1- Geant4 input TG files for gamma simulation

The following is an example of the used input file in the modeling of a silicon glass sample with five holes for 105 WLS fibers for gamma ray simulation. The file contains the definitions of the glass sample, the optical grease, the WLS fibers, the PMT's window and the photocathode. Also, the chosen physics list, ^{60}Co source, visualization macro commands, and the command to create a Root output file.

```
:MIXT_BY_NATOMS SiO2Glass 2.44 2
Si 1
O 2

:MIXT_BY_NATOMS SiO2PMT 2.203 2
Si 1
O 2

:MIXT_BY_NATOMS SiliconeOpticalGrease 1.06 4
C 2
H 6
O 1
Si 1

:MIXT_BY_NATOMS Fiber_Core_Polystyrene 1.05 2
C 8
H 8


// default unit of length is mm
:volu world BOX 1000 1000 1000 G4_AIR
:volu Glass TUBE 0 20 15 SiO2Glass
:volu WLSHolder TUBE 0 3 12.5 SiliconeOpticalGrease
:volu OpticalGrease TUBE 0 25.5 0.25 SiliconeOpticalGrease
:volu Teflon TUBE 20 20.1 15 G4_TEFLON
:volu TeflonCover1 TUBE 0. 20 0.5 G4_TEFLON
:volu TeflonCover2 TUBE 21 25.5 0.5 G4_TEFLON
```

```
:volu PMT TUBE 0. 25.5 80 G4_Galactic
:volu PMTw TUBE 0. 25.5 0.5 SiO2PMT
:volu PhotoCathode TUBE 0. 23 0.25 SiO2PMT
:volu WLSCore BOX 0.5 0.5 12.5 Fiber_Core_Polystyrene
:rotm r000 0 0 0
:place Teflon 1 world r000 0 0 0
:place Glass 2 world r000 0 0 0
:place PMT -3 world r000 0 0 -95.5
:place PMTw 4 PMT r000 0 0 79.5
:place PhotoCathode 5 PMT r000 0 0 73.75
:place TeflonCover1 6 world r000 0 0 15.5
:place TeflonCover2 7 world r000 0 0 -14.5
:place WLSHolder 8 Glass r000 0 0 -2.5
:place WLSHolder 9 Glass r000 11.8 0 -2.5
:place WLSHolder 10 Glass r000 -11.8 0 -2.5
:place WLSHolder 11 Glass r000 0 11.8 -2.5
:place WLSHolder 12 Glass r000 0 -11.8 -2.5
:place OpticalGrease 13 world r000 0 0 -15.25
:place WLSCore -70 WLSHolder r000 0 0 0
:place WLSCore -90 WLSHolder r000 1 0 0
:place WLSCore -11 WLSHolder r000 2 0 0
:place WLSCore -13 WLSHolder r000 -1 0 0
:place WLSCore -15 WLSHolder r000 -2 0 0
:place WLSCore -17 WLSHolder r000 0 1 0
:place WLSCore -19 WLSHolder r000 0 2 0
:place WLSCore -21 WLSHolder r000 0 -1 0
:place WLSCore -23 WLSHolder r000 0 -2 0
:place WLSCore -25 WLSHolder r000 1 1 0
:place WLSCore -27 WLSHolder r000 1 2 0
:place WLSCore -29 WLSHolder r000 1 -1 0
:place WLSCore -31 WLSHolder r000 1 -2 0
:place WLSCore -33 WLSHolder r000 2 1 0
:place WLSCore -35 WLSHolder r000 2 -1 0
:place WLSCore -37 WLSHolder r000 -1 1 0
:place WLSCore -39 WLSHolder r000 -1 -1 0
:place WLSCore -41 WLSHolder r000 -1 2 0
:place WLSCore -43 WLSHolder r000 -1 -2 0
:place WLSCore -45 WLSHolder r000 -2 1 0
:place WLSCore -47 WLSHolder r000 -2 -1 0
```

```
// optical properties of OpticalGrease
:prop SiliconeOpticalGrease

 photon_energies 64 6.1992*eV 3.451*eV 3.423*eV 3.376*eV 3.331*eV
3.287*eV 3.244*eV 3.202*eV 3.161*eV 3.122*eV 3.083*eV 3.068*eV
3.053*eV 3.038*eV 3.023*eV 3.008*eV 2.972*eV 2.937*eV 2.903*eV
2.869*eV 2.837*eV 2.804*eV 2.773*eV 2.743*eV 2.713*eV 2.683*eV
2.678*eV 2.655*eV 2.632*eV 2.627*eV 2.621*eV 2.599*eV 2.588*eV
2.578*eV 2.556*eV 2.535*eV 2.525*eV 2.485*eV 2.465*eV 2.446*eV
2.427*eV 2.408*eV 2.389*eV 2.371*eV 2.353*eV 2.335*eV 2.318*eV
2.301*eV 2.284*eV 2.267*eV 2.251*eV 2.235*eV 2.219*eV 2.203*eV
2.187*eV 2.172*eV 2.157*eV 2.142*eV 2.127*eV 2.113*eV  2.099*eV
2.085*eV 2.071*eV 1.7712*eV

RINDEX 1.46 1.46 1.46 1.46 1.46 1.46 1.46 1.46 1.46 1.46 1.46 1.46 1.46 1.46
1.46 1.46 1.46 1.46 1.46 1.46 1.46 1.46 1.46 1.46 1.46 1.46 1.46 1.46 1.46 1.46
1.46 1.46 1.46 1.46 1.46 1.46 1.46 1.46 1.46 1.46 1.46 1.46 1.46 1.46 1.46 1.46
1.46 1.46 1.46 1.46 1.46 1.46 1.46 1.46 1.46 1.46 1.46 1.46 1.46 1.46 1.46 1.46
1.46 1.46

ABSLENGTH 0.7*cm 0.7*cm 0.7*cm 0.7*cm 0.7*cm 0.7*cm 0.7*cm 0.7*cm
0.7*cm 0.7*cm 0.7*cm 0.7*cm 0.7*cm 0.7*cm 0.7*cm 0.7*cm 0.7*cm 0.7*cm
0.7*cm 0.7*cm 0.7*cm 0.7*cm 0.7*cm 0.7*cm 0.7*cm 0.7*cm 0.7*cm 0.7*cm
0.7*cm 0.7*cm 0.7*cm 0.7*cm 0.7*cm 0.7*cm 0.7*cm 0.7*cm 0.7*cm 0.7*cm
0.7*cm 0.7*cm 0.7*cm 0.7*cm 0.7*cm 0.7*cm 0.7*cm 0.7*cm 0.7*cm 0.7*cm
0.7*cm 0.7*cm 0.7*cm 0.7*cm 0.7*cm 0.7*cm 0.7*cm 0.7*cm 0.7*cm 0.7*cm
0.7*cm 0.7*cm 0.7*cm 0.7*cm 0.7*cm 0.7*cm


:prop Fiber_Core_Polystyrene

WLSTIMECONSTANT 2.7*ns

photon_energies 62 3.451*eV 3.423*eV 3.376*eV 3.331*eV 3.287*eV 3.244*eV
3.202*eV 3.161*eV 3.122*eV 3.083*eV 3.068*eV 3.053*eV 3.038*eV
3.023*eV 3.008*eV 2.972*eV 2.937*eV 2.903*eV 2.869*eV 2.837*eV
2.804*eV 2.773*eV 2.743*eV 2.713*eV 2.683*eV 2.678*eV 2.655*eV
2.632*eV 2.627*eV 2.621*eV 2.599*eV 2.588*eV 2.578*eV 2.556*eV
2.535*eV 2.525*eV 2.485*eV 2.465*eV 2.446*eV 2.427*eV 2.408*eV
```

2.389*eV 2.371*eV 2.353*eV 2.335*eV 2.318*eV 2.301*eV 2.284*eV
2.267*eV 2.251*eV 2.235*eV 2.219*eV 2.203*eV 2.187*eV 2.172*eV
2.157*eV 2.142*eV 2.127*eV 2.113*eV 2.099*eV 2.085*eV 2.071*eV

//using polysterene's dispersion formula
RINDEX 1.60 1.60 1.60 1.60 1.60 1.60 1.60 1.60 1.60 1.60 1.60 1.60 1.60 1.60
1.60 1.60 1.60 1.60 1.60 1.60 1.60 1.60 1.60 1.60 1.60 1.60 1.60 1.60 1.60
1.60 1.60 1.60 1.60 1.60 1.60 1.60 1.60 1.60 1.60 1.60 1.60 1.60 1.60 1.60
1.60 1.60 1.60 1.60 1.60 1.60 1.60 1.60 1.60 1.60 1.60 1.60 1.60 1.60 1.60

// emission spectrum
WLSCOMPONENT 0.0 0.0 0.0 0.0 0.0 0.0 0.0 0.0 0.0 0.0 0.0 0.0 0.0 0.0 0.0 0.0
0.0 0.0 0.0 0.0 0.0 0.0 0.0 0.0 0.0 0.05 0.52 1.5 2.2 2.8 6.185 7.28 8.66 9.691 9.98
9.98 9.691 9.278 8.557 7.526 7.01 6.289 5.67 5.155 4.536 4.021 3.608 3.196
2.886 2.577 2.165 1.856 1.752 1.459 1.34 1.186 1.031 0.876 0.835 0.773 0.701
0.536

// Absorblength
WLSABSLENGTH 0.001*nm 0.001*nm 0.001*nm 0.001*nm 0.001*nm
0.001*nm 0.001*nm 0.001*nm 0.001*nm 0.001*nm 0.001*nm 0.001*nm
0.001*nm 0.001*nm 0.001*nm 0.001*nm 0.001*nm 0.001*nm 0.001*nm
0.001*nm 0.001*nm 0.001*nm 0.001*nm 0.001*nm 0.001*nm 0.001*nm 55*cm 55*cm
55*cm 55*cm 55*cm 55*cm 55*cm 55*cm 55*cm 55*cm 55*cm 55*cm 55*cm
55*cm 55*cm 55*cm 55*cm 55*cm 55*cm 55*cm 55*cm 55*cm 55*cm 55*cm
55*cm 55*cm 55*cm 55*cm 55*cm 55*cm 55*cm 55*cm 55*cm 55*cm 55*cm
55*cm 55*cm

// optical properties of the surface between Glass1 & Teflon
:surf Glass2Teflon Glass:1 Teflon:1
  type dielectric_dielectric
  model unified
  finish ground
  sigma_alpha 0.1
  property photon_energies 2 1.7712*eV 6.1992*eV
  REFLECTIVITY 0.99 0.99

// visual effects
:color Glass 0.2 0.4 0.8

```
:color Teflon 0.3 0.3 0.3
:color PMTw 0.8 0.4 0.2
:vis world ON

/physics_lists/select QGSP_BERT_EMZ
/physics_lists/factory/addOptical
/process/optical/processActivation Scintillation false
/process/optical/processActivation OpBoundary
/process/optical/processActivation OpAbsorption
/process/optical/processActivation OpRayleigh false
/process/optical/processActivation OpMieHG false
/process/optical/processActivation Cerenkov
/process/optical/processActivation OpWLS
/run/initialize

# Check Overlapping
/geometry/test/run

/control/alias srcpos "0 0 0"
# gamma 1
/gps/source/intensity 0.998 # 99.80%
/gps/particle gamma
/gps/pos/type Point
/gps/pos/centre {srcpos}
/gps/ang/type iso
/gps/ene/type Mono
/gps/ene/mono 1.173 MeV

# gamma 2
/gps/source/add 0.999 # 99.90%
/gps/particle gamma
/gps/pos/type Point
/gps/pos/centre {srcpos}
/gps/ang/type iso
/gps/ene/type Mono
/gps/ene/mono 1.332 MeV

/control/alias pos "0 0 4.6 cm"
/gps/source/set 0
/gps/position {pos}
```

```
/gps/ang/minphi 0 deg
/gps/ang/maxphi 360 deg
/gps/source/set 1
/gps/position {pos}
/gps/ang/minphi 0 deg
/gps/ang/maxphi 360 deg

# list all sources
/gps/source/list

/vis/open HepRepFile
/vis/drawVolume
#vis/scene/add/axes 0 0 0 10 cm
/vis/scene/add/trajectories
/vis/scene/add/hits

/random/setSeeds 2412 79628

# turn on detailed information about tracking
#/tracking/verbose 2
# run a few events for debugging
/run/beamOn 10
# turn off screen dump for fast simulation
/tracking/verbose 0
/vis/disable
# Output Root Data file
/analysis/setFileName outputWLS5holes
# Print a Summary
/run/verbose 2
#/run/printProgress 10
/run/beamOn 1000000
```

2- Geant4 input TG files for neutron simulation

The following is an example of the used input file in the modeling of a lead glass sample with five holes for 105 WLS fibers for neutron simulation. The file contains the definitions of the glass sample, gadolinium, the optical grease, the WLS fibers, the PMT's window and the photocathode. Also, the chosen physics list, the neutron source, visualization macro commands, and the command to create a Root output file.

```
:MIXT_BY_NATOMS leadGlass 6.22 3
Pb 1
Si 1
O 3

:MIXT_BY_NATOMS SiO2PMT 2.203 2
Si 1
O 2

:MIXT_BY_NATOMS SiO2Photocath 2.203 2
Si 1
O 2

:MIXT_BY_NATOMS SiliconeOpticalGrease 1.06 4
C 2
H 6
O 1
Si 1

:MIXT_BY_NATOMS Fiber_Core_Polystyrene 1.05 2
C 8
H 8

:MIXT_BY_NATOMS Gd2O3 7.407 2
Gd 2
O 3
```

```
// default unit of length is mm
:volu world BOX 2000 2000 2000 G4_AIR
:volu Glass TUBE 0 20 15 leadGlass
:volu Teflon TUBE 20 20.5 15 G4_TEFLON
:volu TeflonCover1 TUBE 0 20 0.5 G4_TEFLON
:volu TeflonCover2 TUBE 20.5 25.5 0.5 G4_TEFLON
:volu OpticalGrease TUBE 0 25.5 0.25 SiliconeOpticalGrease
:volu PMT TUBE 0. 25.5 80 G4_Galactic
:volu PMTw TUBE 0. 25.5 0.5 SiO2PMT
:volu PhotoCathode TUBE 0. 23 0.25 SiO2Photocath
:volu Activator TUBE 0 25 0.005 Gd2O3
:volu Lead BOX 50 100 25 G4_Pb
:volu Container_Lid TUBE 0 300 5 G4_Fe
:volu Container TUBE 280 300 425 G4_Fe
:volu Pipe_Lid TUBE 0 20 5 G4_Fe
:volu Pipe TUBE 15 20 160 G4_Fe
:volu Pipe_Paraffin TUBE 0 15 110 G4_PARAFFIN
:volu Paraffin1 TUBE 20 280 90 G4_PARAFFIN
:volu Paraffin2 TUBE 0 280 260 G4_PARAFFIN
:volu WLSHolder TUBE 0 3 12.5 SiliconeOpticalGrease
:volu WLSCore BOX 0.5 0.5 12.5 Fiber_Core_Polystyrene
:rotm r000 0 0 0
:place Glass 1 world r000 0 0 0
:place Teflon 2 world r000 0 0 0
:place TeflonCover1 3 world r000 0 0 15.5
:place TeflonCover2 4 world r000 0 0 -14.5
:place OpticalGrease 5 world r000 0 0 -15.25
:place PMT 6 world r000 0 0 -95.5
:place PMTw 7 PMT r000 0 0 79.5
:place PhotoCathode 8 PMT r000 0 0 73.75
:place Activator 9 world r000 0 0 16.005
:place Lead 10 world r000 0 0 41.01
:place Container_Lid 11 world r000 0 0 71.01
:place Container 12 world r000 0 0 501.01
:place Pipe_Lid 13 world r000 0 0 81.01
:place Pipe 14 world r000 0 0 246.01
:place Pipe_Paraffin 15 world r000 0 0 196.01
:place Paraffin1 16 world r000 0 0 316.01
:place Paraffin2 17 world r000 0 0 666.01
:place WLSHolder 17 Glass r000 0 0 -2.5
```

```
:place WLSHolder 18 Glass r000 11.8 0 -2.5
:place WLSHolder 19 Glass r000 -11.8 0 -2.5
:place WLSHolder 20 Glass r000 0 11.8 -2.5
:place WLSHolder 21 Glass r000 0 -11.8 -2.5
:place WLSCore -70 WLSHolder r000 0 0 0
:place WLSCore -90 WLSHolder r000 1 0 0
:place WLSCore -11 WLSHolder r000 2 0 0
:place WLSCore -13 WLSHolder r000 -1 0 0
:place WLSCore -15 WLSHolder r000 -2 0 0
:place WLSCore -17 WLSHolder r000 0 1 0
:place WLSCore -19 WLSHolder r000 0 2 0
:place WLSCore -21 WLSHolder r000 0 -1 0
:place WLSCore -23 WLSHolder r000 0 -2 0
:place WLSCore -25 WLSHolder r000 1 1 0
:place WLSCore -27 WLSHolder r000 1 2 0
:place WLSCore -29 WLSHolder r000 1 -1 0
:place WLSCore -31 WLSHolder r000 1 -2 0
:place WLSCore -33 WLSHolder r000 2 1 0
:place WLSCore -35 WLSHolder r000 2 -1 0
:place WLSCore -37 WLSHolder r000 -1 1 0
:place WLSCore -39 WLSHolder r000 -1 -1 0
:place WLSCore -41 WLSHolder r000 -1 2 0
:place WLSCore -43 WLSHolder r000 -1 -2 0
:place WLSCore -45 WLSHolder r000 -2 1 0
:place WLSCore -47 WLSHolder r000 -2 -1 0

// optical properties of OpticalGrease
:prop SiliconeOpticalGrease
  photon_energies 64 6.1992*eV 3.451*eV 3.423*eV 3.376*eV 3.331*eV 3.287*eV
3.244*eV  3.202*eV  3.161*eV  3.122*eV  3.083*eV  3.068*eV  3.053*eV  3.038*eV
3.023*eV  3.008*eV  2.972*eV  2.937*eV  2.903*eV  2.869*eV  2.837*eV  2.804*eV
2.773*eV  2.743*eV  2.713*eV  2.683*eV  2.678*eV  2.655*eV  2.632*eV  2.627*eV
2.621*eV  2.599*eV  2.588*eV  2.578*eV  2.556*eV  2.535*eV  2.525*eV  2.485*eV
2.465*eV  2.446*eV  2.427*eV  2.408*eV  2.389*eV  2.371*eV  2.353*eV  2.335*eV
2.318*eV  2.301*eV  2.284*eV  2.267*eV  2.251*eV  2.235*eV  2.219*eV  2.203*eV
2.187*eV 2.172*eV 2.157*eV 2.142*eV 2.127*eV 2.113*eV  2.099*eV 2.085*eV
2.071*eV 1.7712*eV
  RINDEX 1.46 1.46 1.46 1.46 1.46 1.46 1.46 1.46 1.46 1.46 1.46 1.46 1.46 1.46 1.46
1.46 1.46 1.46 1.46 1.46 1.46 1.46 1.46 1.46 1.46 1.46 1.46 1.46 1.46 1.46 1.46 1.46
```

1.46 1.46 1.46 1.46 1.46 1.46 1.46 1.46 1.46 1.46 1.46 1.46 1.46 1.46 1.46 1.46 1.46 1.46 1.46 1.46 1.46 1.46 1.46 1.46 1.46 1.46 1.46 1.46 1.46 1.46 1.46

ABSLENGTH 7.0*mm

:prop Fiber_Core_Polystyrene
WLSTIMECONSTANT 2.7*ns

photon_energies 62 3.451*eV 3.423*eV 3.376*eV 3.331*eV 3.287*eV 3.244*eV 3.202*eV 3.161*eV 3.122*eV 3.083*eV 3.068*eV 3.053*eV 3.038*eV 3.023*eV 3.008*eV 2.972*eV 2.937*eV 2.903*eV 2.869*eV 2.837*eV 2.804*eV 2.773*eV 2.743*eV 2.713*eV 2.683*eV 2.678*eV 2.655*eV 2.632*eV 2.627*eV 2.621*eV 2.599*eV 2.588*eV 2.578*eV 2.556*eV 2.535*eV 2.525*eV 2.485*eV 2.465*eV 2.446*eV 2.427*eV 2.408*eV 2.389*eV 2.371*eV 2.353*eV 2.335*eV 2.318*eV 2.301*eV 2.284*eV 2.267*eV 2.251*eV 2.235*eV 2.219*eV 2.203*eV 2.187*eV 2.172*eV 2.157*eV 2.142*eV 2.127*eV 2.113*eV 2.099*eV 2.085*eV 2.071*eV

//using polysterene's dispersion formula
RINDEX 1.60 1.60 1.60 1.60 1.60 1.60 1.60 1.60 1.60 1.60 1.60 1.60 1.60 1.60 1.60 1.60 1.60 1.60 1.60 1.60 1.60 1.60 1.60 1.60 1.60 1.60 1.60 1.60 1.60 1.60 1.60 1.60 1.60 1.60 1.60 1.60 1.60 1.60 1.60 1.60 1.60 1.60 1.60 1.60 1.60 1.60 1.60 1.60 1.60 1.60 1.60 1.60 1.60 1.60 1.60 1.60 1.60 1.60 1.60 1.60 1.60 1.60

// emission spectrum
WLSCOMPONENT 0.0 0.0 0.0 0.0 0.0 0.0 0.0 0.0 0.0 0.0 0.0 0.0 0.0 0.0 0.0 0.0 0.0 0.0 0.0 0.0 0.0 0.0 0.0 0.0 0.0 0.05 0.52 1.5 2.2 2.8 6.185 7.28 8.66 9.691 9.98 9.98 9.691 9.278 8.557 7.526 7.01 6.289 5.67 5.155 4.536 4.021 3.608 3.196 2.886 2.577 2.165 1.856 1.752 1.459 1.34 1.186 1.031 0.876 0.835 0.773 0.701 0.536

// Absorblength
WLSABSLENGTH 0.001*nm

```
0.001*nm 0.001*nm 0.001*nm 55*cm 55*cm 55*cm 55*cm 55*cm 55*cm 55*cm
55*cm 55*cm 55*cm 55*cm 55*cm 55*cm 55*cm 55*cm 55*cm 55*cm 55*cm
55*cm 55*cm 55*cm 55*cm 55*cm 55*cm 55*cm 55*cm 55*cm 55*cm 55*cm
55*cm 55*cm 55*cm 55*cm 55*cm 55*cm 55*cm 55*cm


// optical properties of the surface between Glass & Teflon
:surf Glass2Teflon Glass:1 Teflon:1
  type dielectric_dielectric
  model unified
  finish ground
  sigma_alpha 0.1
  property photon_energies 2 1.7712*eV 6.1992*eV
  REFLECTIVITY 0.99 0.99

// optical properties of the surface between Glass & TeflonCover1
:surf Glass2TeflonCover1 Glass:1 TeflonCover1:1
  type dielectric_dielectric
  model unified
  finish ground
  sigma_alpha 0.1
  property photon_energies 2 1.7712*eV 6.1992*eV
  REFLECTIVITY 0.99 0.99

:vis world ON

/physics_lists/select FTFP_BERT_HP
/physics_lists/factory/addOptical
/process/optical/processActivation Scintillation false
/process/optical/processActivation OpBoundary
/process/optical/processActivation OpAbsorption
/process/optical/processActivation OpRayleigh false
/process/optical/processActivation OpMieHG false
/process/optical/processActivation Cerenkov
/process/optical/processActivation OpWLS
/run/initialize

# Check Overlapping
/geometry/test/run
```

```
/gps/source/set 0
/gps/pos/type Volume
/gps/pos/shape Cylinder
/gps/pos/radius 1.5 cm
/gps/pos/halfz 5 cm
/gps/number 1

#/gps/List
/gps/source/list

# Neutron Spectrum
/gps/particle neutron

/gps/position 0 0 35.601 cm
/gps/direction 0 0 -1
/gps/ene/type User
/gps/hist/type energy

/gps/hist/point 0.80 0.51163
/gps/hist/point 0.93 0.65116
/gps/hist/point 1.06 0.61628
/gps/hist/point 1.20 0.53488
/gps/hist/point 1.40 0.51163
/gps/hist/point 1.60 0.50233
/gps/hist/point 1.80 0.51163
/gps/hist/point 2.00 0.56744
/gps/hist/point 2.13 0.62791
/gps/hist/point 2.40 0.62791
/gps/hist/point 2.66 0.68837
/gps/hist/point 2.93 0.82791
/gps/hist/point 3.07 0.92093
/gps/hist/point 3.20 1.00000
/gps/hist/point 3.60 0.95349
/gps/hist/point 3.73 0.88372
/gps/hist/point 3.87 0.84651
/gps/hist/point 4.13 0.85349
/gps/hist/point 4.40 0.90698
/gps/hist/point 4.80 0.85349
/gps/hist/point 5.20 0.79070
/gps/hist/point 5.40 0.65116
```

```
/gps/hist/point 5.60 0.55814
/gps/hist/point 6.00 0.51163
/gps/hist/point 6.27 0.47442
/gps/hist/point 6.60 0.46512
/gps/hist/point 6.80 0.46512
/gps/hist/point 7.20 0.46977
/gps/hist/point 7.80 0.45581
/gps/hist/point 8.26 0.32558
/gps/hist/point 8.80 0.22791
/gps/hist/point 9.20 0.17674
/gps/hist/point 9.73 0.13953
/gps/hist/point 10.27 0.08837
/gps/hist/point 10.80 0.04651
/gps/hist/point 11.20 0.02326
/gps/hist/point 11.80 0.00000

/vis/open HepRepFile
/vis/drawVolume
#vis/scene/add/axes 0 0 0 10 cm
/vis/scene/add/trajectories
/vis/scene/add/hits

/random/setSeeds 2412 79628

# turn on detailed information about tracking
#/tracking/verbose 2
# run a few events for debugging
/run/beamOn 10
# turn off screen dump for fast simulation
/tracking/verbose 0
/vis/disable
# Output Root Data file
/analysis/setFileName outputPbO+SiO2+Gd2O3+105WLS(Center)
# Print a Summary
/run/verbose 2
/run/printProgress 1000
/run/beamOn 1000000
```

3- Output Root File Histogram

The following is an example of building a Cherenkov light histogram containing several spectra from several Root files.

```
{
    gStyle->SetOptStat(0); // turn off statistical box
    gStyle->SetTitleSize(0.05, "xy");
    gStyle->SetPadBottomMargin(0.11);
    gStyle->SetLabelSize(0.05, "xy");
    gStyle->SetTitleOffset(0.7, "y");

    TChain *t1 = new TChain("t");
    t1->Add("outputNoWLS.root");

    TH1F *h1 = new TH1F("h1",";Wavelength [nm];# Cherenkov Photons", 100, 100, 800);
    t1->Draw("(6.626E-34*3E8*1000000)/(k*1.6E-19)>>h1", "pro==2021 && k<0.008");

    TChain *t2 = new TChain("t");
    t2->Add("outputWLS1holeWithCenter.root");
```

```
TH1F *h2 = new TH1F("h2",";Wavelength [nm];# Cherenkov Photons", 100, 100, 800);
t2->Draw("(6.626E-34*3E8*1000000)/(k*1.6E-19)>>h2", "pro==2021 && k<0.008");

TChain *t3 = new TChain("t");
t3->Add("outputWLS1holeNoCenter.root");

TH1F *h3 = new TH1F("h3",";Wavelength [nm];# Cherenkov Photons", 100, 100, 800);
t3->Draw("(6.626E-34*3E8*1000000)/(k*1.6E-19)>>h3", "pro==2021 && k<0.008");

TChain *t4 = new TChain("t");
t4->Add("outputWLS2holesWithCenter.root");

TH1F *h4 = new TH1F("h4",";Wavelength [nm];# Cherenkov Photons", 100, 100, 800);
t4->Draw("(6.626E-34*3E8*1000000)/(k*1.6E-19)>>h4", "pro==2021 && k<0.008");

TChain *t5 = new TChain("t");
t5->Add("outputWLS3holesWithCenter.root");
```

```
TH1F *h5 = new TH1F("h5",";Wavelength [nm];# Cherenkov Photons", 100, 100, 800);
t5->Draw("(6.626E-34*3E8*1000000)/(k*1.6E-19)>>h5", "pro==2021 && k<0.008");

TChain *t6 = new TChain("t");
t6->Add("outputWLS4holesWithCenter.root");

TH1F *h6 = new TH1F("h6",";Wavelength [nm];# Cherenkov Photons", 100, 100, 800);
t6->Draw("(6.626E-34*3E8*1000000)/(k*1.6E-19)>>h6", "pro==2021 && k<0.008");

TChain *t7 = new TChain("t");
t7->Add("outputWLS5holes.root");

TH1F *h7 = new TH1F("h7",";Wavelength [nm];# Cherenkov Photons", 100, 100, 800);
t7->Draw("(6.626E-34*3E8*1000000)/(k*1.6E-19)>>h7", "pro==2021 && k<0.008");

        h2->SetLineColor(kRed);
```

```
        h3->SetLineColor(kGreen);
        h4->SetLineColor(kBlack);
        h5->SetLineColor(kViolet);
        h6->SetLineColor(kGreen);
        h7->SetLineColor(kOrange);
        h2->Draw();
        h6->Draw("same");
        h5->Draw("same");
        h4->Draw("same");
        h3->Draw("same");
        h1->Draw("same");
        h7->Draw("same");
        TLegend *leg = new TLegend(0.2,0.7,0.5,0.9);
        leg->AddEntry(h1, "N_{No WLS}", "l");
        leg->AddEntry(h2, "N_{WLS-Center}=21", "l");
        leg->AddEntry(h3, "N_{WLS-off Center}=21", "l");
        leg->AddEntry(h4, "N_{WLS-Center}=42", "l");
        leg->AddEntry(h5, "N_{WLS-Center}=63", "l");
        leg->AddEntry(h6, "N_{WLS-Center}=84", "l");
        leg->AddEntry(h7, "N_{WLS-Center}=105", "l");
        leg->Draw();
        gPad->Print("k2.png");
}
```